Error Growth in Position Estimation from Noisy Relative Pose Measurements

Joseph Knuth and Prabir Barooah*

Abstract

We examine how the estimation error grows with time when a mobile robot estimates its location from relative pose measurements without global position or orientation sensors. We show that in both 2-D or 3-D space, both the bias and variance of the position estimation error grows at most linearly with time (or distance traversed) asymptotically. The bias is crucially dependent on the trajectory of the robot. Conclusions on the asymptotic growth rate of the bias continue to hold even with unbiased measurements or error-free translation measurements. Exact formulas for the bias and the variance of the position estimation error are provided for two specific 2-D trajectories- straight line and periodic. Experiments with a P3-DX wheeled robot and Monte-Carlo simulations are provided to verify the theoretical predictions. A method to reduce the bias is proposed based on the lessons learned.

Keywords: Localization, position estimation, error growth, autonomous vehicle, vision-based estimation, dead reckoning error

1. Introduction

Localization without GPS is a key capability for autonomous robots, since there are many situations in which GPS signals are either unavailable or only intermittently available. These include operation in urban canyons and tunnels, inside buildings, under water, and extra-planetary exploration. In such a situation, localization with respect to an initial position is typically performed using a combination of sensors that are used to measure relative motion between two successive time instants, and then chaining them together. Inertial sensors (gyroscopes and accelerometers), vision-based sensors (cameras, LIDARs, etc) and joint encoders (in case of ground vehicles) are examples of sensors that can be used to obtain such measurements. Apart from robotic platforms, such localization is also of relevance to human wearable systems [1], personal navigation devices [2], and robot end-effector position estimation [3].

In this paper we examine the growth rate in the position estimation error of a robot that cannot directly measure either its global position or its global orientation. Specifically, we analyze the bias and the variance of the error. The robot is equipped with sensors that allows it to measure the relative pose (position and orientation) between its coordinate frames at two successive time instants, but not sensors that can measure its absolute pose with respect to a global coordinate frame. That is, the robot may have sensors such as wheel odometers, IMUs, and cameras, but does not have sensors such as GPS and compasses. The absolute position has to be estimated from the noisy relative pose measurements.

When relative pose measurements obtained from sensors are concatenated to form an estimate of the robot's position in a global frame, errors in individual measurements accumulate. Over long time horizons, the resulting location estimates may become quite poor. Though this is well recognized, a rigorous analysis of the asymptotic growth rate seems to be lacking. Olson et. al. [4] states that without a global orientation sensor, the error grows super-linearly with distance, and presents experimental evidence. They also state that position estimation error will grow as $O(s^{3/2})$, where s is the distance travelled. A number of papers have claimed, without proof, that the position estimation error grows super-linearly with distance or time in the absence of an absolute orientation sensor [5, 6, 7, 8, 9, 10]. It is also not clear what is meant by "error" in these references, whether it is the mean, variance or some other measure. A parametric statistical model of the 2-norm of the position estimation error is proposed in [11], whose parameters have to be fitted from measured error.

We show in this paper that the asymptotic growth rates of both the bias the variance of the position estimation error are upper bounded by linear functions of time. Thus, even without an absolute orientation sensor, the error growth (both bias and variance) is at most linear. We also show that the variance growth rate is lower bounded by a linear function of time as well, if the variance of the translation measurement is sufficiently large. Our analysis also provides insight into the mechanism of error growth, particularly its bias, that does not seem to have been recognized so far. In particular, we show that the expected value of the robot's position estimate converges to a point

*Corresponding author
Email address: knuth,pbarooah@ufl.edu (Joseph Knuth and Prabir Barooah)

irrespective of whether the robot stays in a bounded region for all time or not. An outcome of this fact is that the growth in the bias depends crucially on the type of path the robot traverses even though the robot does not have - and does not use - information about its trajectory. The bias will be bounded or unbounded depending only on whether the robot stays within a bounded region or not. In addition, the asymptotic trends for the bias hold even if the measurements of relative translation and rotation are unbiased. In fact, they hold even if the relative translation measurements are completely error-free. The bias in the translation *measurements* that arise from vision-based sensors has been a topic of research [12, 13]. However, the fact that large position estimation bias may occur even when all measurements are unbiased has not been emphasized in the literature.

The results mentioned above, which are stated in Theorem 1 of the paper, are for the general d-D case: the robot's pose is an element of $SE(d)$, $d \in \{2, 3\}$. For two special trajectories in 2-D, namely straight line and periodic, we provide exact formulas for the bias and the variance of the position estimation error. Analysis of the 2-D case is more tractable than the 3-D case since 2-D rotation matrices commute. From the expressions we obtain, we see that the bias and variance do indeed appear to grow faster than linearly with time for small time intervals. The linear asymptotic trend is visible only when time is sufficiently large. These results are verified numerically through Monte-Carlo simulations. We also provide experimental verification of the periodic case through experiments conducted with a Pioneer P3-DX robot equipped with a vision-based sensor and a wheel odometer.

By establishing these bounds through rigorous analysis, we clarify the misconceptions that are prevalent in the literature on the scaling laws of the error with time. Another outcome of the analysis carried out here is a method for reducing the bias in the position estimates. The method is suggested naturally by the lessons learned during the analysis. Preliminary results are included in the paper; with a more thorough investigation of the method planned for the future.

Other applications of our results lie in collaborative localization of a group of robots. The collaborative localization algorithms reported in [14, 15, 16, 17] fuse the measurement of the change in pose of a robot between two time instants, which we call *inter-time relative measurements*, with the measurement of relative pose between two robots taken at the second of these two time instants, which we call *inter-robot measurements*. Figure 1 provides an illustration of these two types of measurements. The results of this paper, which are for a single robot, can be used to determine appropriate weights on the inter-robot and inter-time measurements in collaborative algorithms. An inter-time measurement is in fact computed by concatenating a number of relative pose measurements obtained at intermediate time instants. Since the autonomous robots are deployed in obstacle rich environments, the time interval between two successive inter-robot measurements is likely to be long. The inter-time measurements therefore have much larger error than the inter-robot measurements. As a result, the weights have to be chosen so that highly noisy measurements are not weighted equally with less noisy ones. Usually the weights are chosen to be inversely proportional to the variances. When the sensor characteristics are not accurately known, knowledge of error variance growth over time can be used to determine appropriate weights. For instance, since the variance growth rate is linear in time, a reasonable estimate of the variance of a inter-time measurement is equal to the time duration of that measurement, while that on a inter-robot measurement is one; see Figure 1 for an example. An additional use of the asymptotic error growth rate for a single robot is that it serves as a benchmark for collaborative localization algorithms. A collaborative algorithm capable of reducing the asymptotic trend of the error growth - over a single robot case - would be of particular interest. An algorithm that can reduce the error by a constant factor but not its asymptotic trend, in contrast, is of less interest. We believe the present study will be useful for this line of research in the future.

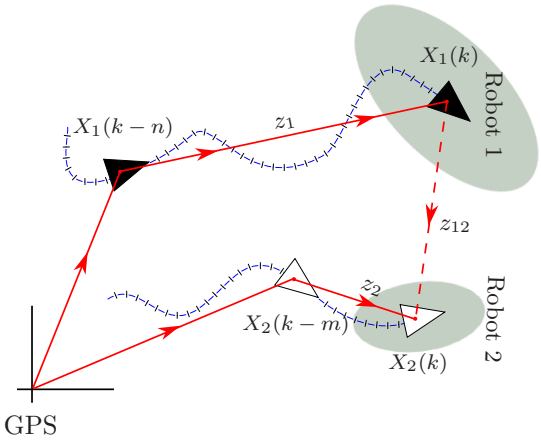

Figure 1: Motivating example: robots performing collaborative localization using inter-robot measurement when GPS is only intermittently available. Inter-time measurements such as z_1, z_2 are combined with inter-robot measurement z_{12}, along with past estimates of the robots' positions. GPS measurements were last obtained by robot 1 and 2 at time $k-n$ and $k-m$, respectively. Appropriate weights have to be assigned on the pose measurements z_1, z_2, z_{12} based on their variances before they are combined for cooperative localization. When an accurate characterization of the robots' onboard sensors is not available, a good choice for the variances of the measurements z_1, z_2 and z_{12} is n, m and 1. This choice is suggested by the results in this paper, in particular, the result that the growth of variance in self-localization is linear in time. Prior results in the literature would lead to a choice of $n^{3/2}, m^{3/2}$ and 1.

The rest of the paper is organized as follows. Section 1.1 discusses some related work. Section 2 precisely formulates the problem under study, and Section 3 states the main results. Most of the proofs are in the appendix at the end of the paper. Simulation verification is presented in Section 4 and experimental verification is presented in

Section 5. A method to reduce the bias is position error is given in section 6. The paper ends with a discussion of the results in Section 7.

1.1. Related work

The papers by Smith and Cheesman [3], Su and Lee [18], and Wang and Chirikjian [19] derived recursive expressions for the covariance of the pose estimation error by assuming the errors are small, so that a first order approximation of the BCH (Baker-Campbell-Hausdorff) formula is valid. Recently, Wang and Chirikjian [20] developed a recursive formula for the covariance of the pose estimation error that retains the second order terms in the BCH formula. The paper [21] examines dead recking error's probability density function for non-holonomic robots in 2-D. The work that comes closest to ours in spirit is [11], which proposed a parametric statistical model of the 2-norm of the position estimation error. Some of the parameters have to be fitted from measured error. However, the works mentioned above do not analyze asymptotic behavior of the error's mean and variance.

A related body of literature deals with problem of developing state estimation techniques for systems whose states, as well as the noisy measurements, are in $SO(3)$ or $SE(3)$ (see [22, 23] and references therein). The problem of position estimation of a mobile robot with noisy relative pose measurements between successive frames - one that is central to this paper - falls into this category. However, our aim is not to develop an estimation technique, but to examine the growth of error in the position estimate when successive noisy relative pose measurements are chained together to obtain a global pose estimate.

2. Problem statement

We measure time with a discrete index $k = 0, 1, \ldots$. Sensors used for relative localization of autonomous vehicles yield an estimate of the position and orientation of the vehicle at time k relative to that in the previous time instant, $k-1$. That is, they produce an estimate of the *relative pose* between frames attached to the robot at two successive time instants. Let $\mathbf{R}_{k+1}^{k}$ be the rotation between the local frames attached to the robot's body at time k and $k+1$. That is, if $\mathbf{u}^k$ is a vector expressed in the vehicle's frame at time k and $\mathbf{u}^{k-1}$ is the same vector expressed in the vehicle's frame at time $k-1$, then $\mathbf{u}^{k-1} = \mathbf{R}_k^{k-1}\,\mathbf{u}^k$. This notation is adopted from [24]. We will refer to the frame that is attached to the vehicle at time k as the "frame k". Similarly, let $\mathbf{t}_{i,j}^{k}$ be the relative translation from the frame i to the frame j, expressed in the frame k. The rotation $\mathbf{R}_k^{k-1} \in \mathrm{SO}(d)$ is usually expressed as a $d \times d$ matrix for $d \in \{2, 3\}$, while $\mathbf{t}_{i,j}^{k}$ is a vector in $\mathbb{R}^d$. Without loss of generality, the coordinate frame that is attached to the robot's body at the initial time $k = 0$ is used as the global coordinate frame. We denote the rotation from frame k to the global coordinate frame (frame 0) by $\mathbf{R}_k^0$. Similarly, the translation from frame $k-1$ to k expressed in the global coordinate frame is denoted by $\mathbf{t}_{k-1,k}^{0}$. The position of the robot at any given time n is the vector $\mathbf{t}_{0,n}^{0}$.

With relative pose sensors such as cameras, inertial sensors, and wheel odometers, the measurements available at time k are estimates of the relative translation from $k-1$ to frame k expressed in frame k, i.e., of $\mathbf{t}_{k-1,k}^{k}$, and the rotation between the frames $k-1$ and k. i.e., of $\mathbf{R}_k^{k-1}$. The translation from $k-1$ to k, for $k \geq 1$, expressed in the global coordinate frame is

$$\mathbf{t}_{k-1,k}^{0} = \mathbf{R}_k^0\,\mathbf{t}_{k-1,k}^{k}, \quad \text{where} \quad \mathbf{R}_k^0 = \mathbf{R}_1^0\,\mathbf{R}_2^1 \ldots \mathbf{R}_k^{k-1}.$$

An example of a robots path along with its corresponding relative pose measurements can be seen in Figure 2. Estimates are denoted by hats on top of the corresponding symbols, and errors by tildes, so that $\hat{\mathbf{R}}_k^{k-1}$ and $\hat{\mathbf{t}}_{k-1,k}^{k}$ are the noisy estimates of $\mathbf{R}_k^{k-1}$ and $\mathbf{t}_{k-1,k}^{k}$, and the corresponding errors $\tilde{\mathbf{R}}_k^{k-1}$ and $\tilde{\mathbf{t}}_{k-1,k}^{k}$ are defined as

$$\begin{aligned} \tilde{\mathbf{R}}_k^{k-1} &:= (\mathbf{R}_k^{k-1})^{-1}\,\hat{\mathbf{R}}_k^{k-1}, \\ \tilde{\mathbf{t}}_{k-1,k}^{k} &:= \hat{\mathbf{t}}_{k-1,k}^{k} - \mathbf{t}_{k-1,k}^{k}. \end{aligned} \tag{1}$$

The absolute position of the robot at time k is determined by adding the relative position measurements, after expressing them all in the global coordinate frame. The measurement of the translation from frame $k-1$ to k expressed in the global coordinate frame, which is denoted by $\hat{\mathbf{t}}_{k-1,k}^{0}$, is

$$\hat{\mathbf{t}}_{k-1,k}^{0} := \hat{\mathbf{R}}_k^{0}\,\hat{\mathbf{t}}_{k-1,k}^{k}, \tag{2}$$

where $\hat{\mathbf{R}}_k^{0}$ is an estimate of $\mathbf{R}_k^0$, which is computed from the relative rotation estimates as

$$\hat{\mathbf{R}}_k^{0} = \prod_{i=1}^{k} \hat{\mathbf{R}}_i^{i-1}. \tag{3}$$

Finally, the estimate of the position at time n in the global coordinate frame 0 is obtained by adding the relative translation estimates after transforming them to frame 0:

$$\hat{\mathbf{t}}_{0,n}^{0} := \sum_{k=1}^{n} \hat{\mathbf{t}}_{k-1,k}^{0}. \tag{4}$$

The error between the estimated position and the true position at time n is

$$\mathbf{e}(n) := \mathbf{t}_{0,n}^{0} - \hat{\mathbf{t}}_{0,n}^{0}. \tag{5}$$

The goal of this paper is to study how the mean and covariance of the position estimation error $\mathbf{e}(n)$ *scales with the time index* n. If the robot's speed is upper and lower bounded by two constants, then the asymptotic trends

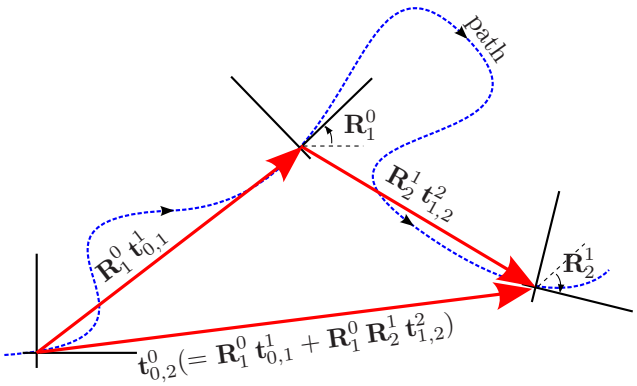

Figure 2: A figure to explain the notation: a robot's path (shown in dashed blue line) in 2-D and associated relative poses between time instants. $\mathbf{t}_{k-1,k}^0$ is the translation between the frames $k-1$ and k, expressed in the global frame 0, and $\mathbf{t}_{k-1,k}^k$ is the same vector expressed in the local frame k. The matrix $\mathbf{R}_k^0$ is the rotation between frame 0 and k, so that $\mathbf{R}_k^0\mathbf{t}_{k-1,k}^k$ is the translation from $k-1$ to k expressed in the global frame 0.

with time are equivalent to those with distance travelled. Therefore we only study scaling with the time index n.

The straight-forward dead-reckoning formula (4) may not be used in practice. Typically a filtering-based algorithm is used to fuse relative pose measurements with the predictions of a model of the robot's motion. There are many variations possible in terms of assumed model, states and input measurements; see [25] for a comparison among some of them. This renders examining the mechanism of error propagation and establishing asymptotic growth rates of such algorithms intractable. Therefore we adopt the simple dead-reckoning model that still captures the essential features of localization from relative pose measurements. We wish to emphasize that the estimation error resulting from the estimation method described above will have the same asymptotic trend as that of a filtering technique that uses a kinematic model of the robot motion. The reason is that a kinematic model essentially produces an independent noisy measurement of the relative pose. Thus, our investigations are useful in analyzing asymptotic performance of a wider class of estimation techniques. One situation where our model is *not* appropriate is when vision-based loop-closure is used to augment localization [26]. We focus on situations where loop closure is not applicable, e.g., an unmanned aerial vehicle flying in an expansive environment so that it may not come back to its earlier positions.

To state the assumptions on measurement error statistics, we establish a few conventions. A rotation matrix $R \in SO(3)$, where the special orthogonal group $SO(3)$ is the set of 3×3 real orthogonal matrices with unit determinant, can be represented by the exponential map: $R = e^{\omega^s}$, where ω^s is the 3×3 skew-symmetric matrix corresponding to the vector $\omega \in \mathbb{R}^3$ [27, Chapter 2]. A matrix in $SO(2)$ is uniquely specified by an angle $\theta \in [-\pi,\ \pi)$. A random rotation matrix $\mathbf{R} \in$ SO(3) (resp. $SO(2)$) can therefore be specified by a random vector $\boldsymbol{\omega} \in \mathbb{R}^3$ (resp. a scalar r.v. θ). We say that two random rotation matrices $\mathbf{R}_1, \mathbf{R}_2 \in SO(3)$ are independent if their corresponding $\boldsymbol{\omega}_1$ and $\boldsymbol{\omega}_2$ are independent random vectors. For $SO(2)$, independence of rotations is defined as the independence of the scalar random variables θ_1, θ_2 that uniquely determine them. If $\mathbf{R}_1$ and $\mathbf{R}_2$ are independent, every entry of the matrix $\mathbf{R}_1$ is independent of every entry of $\mathbf{R}_2$. Similarly, we say that a rotation $\mathbf{R}_1 \in SO(3)$ (resp., $SO(2)$) and a random vector $\mathbf{t} \in \mathbb{R}^3$ (resp. $\mathbb{R}^2$) are independent if $\boldsymbol{\omega}_1$ (resp., θ) and $\mathbf{t}$ are independent. In this case, too, every entry of $\mathbf{t}$ is independent of every entry of $\mathbf{R}$.

In this paper, we use $\mathrm{E}[\mathbf{R}]$ (for a random rotation matrix $\mathbf{R}$) to denote the matrix whose i,j-th entry is $\mathrm{E}[(\mathbf{R})_{i,j}]$, i.e., the expected value of the i,j-th entry of $\mathbf{R}$. As a result of this convention, if $\mathbf{R}_1 \in SO(d)$ is independent of $\mathbf{R}_2 \in SO(d)$ and of $\mathbf{t} \in \mathbb{R}^3$, then $\mathrm{E}[\mathbf{R}_1\mathbf{R}_2] = \mathrm{E}[\mathbf{R}_1]\,\mathrm{E}[\mathbf{R}_2]$ and $\mathrm{E}[\mathbf{R}_1\mathbf{t}] = \mathrm{E}[\mathbf{R}_1]\,\mathrm{E}[\mathbf{t}]$.

In the sequel, $\mathrm{Tr}\,[\,\cdot\,]$ stands for trace of a matrix, and $\|\cdot\|_q$ denotes the (induced) q-norm of a (matrix) vector. When the subscript is omitted, it denotes the (induced) 2-norm.

We state the following assumptions for use in the rest of the paper.

Assumption 1. 1. *The robot's speed is uniformly bounded. More specifically, there exists a constant $\tau > 0$ such that $\|\mathbf{t}_{k-1,k}^k\| \le \tau$.*

2. *The translation measurement errors $\tilde{\mathbf{t}}_{k-1,k}^k$ form a sequence of independent random vectors, with mean $\mathbf{b}_k := \mathrm{E}[\tilde{\mathbf{t}}_{k-1,k}^k]$ and covariance $\mathbf{P}_k := Cov(\tilde{\mathbf{t}}_{k-1,k}^k, \tilde{\mathbf{t}}_{k-1,k}^k)$ that are uniformly bounded. That is, there exist scalar constants b, $\underline{p}$, $\overline{p}$ such that $0 \le \|\mathbf{b}_k\| \le b$ and $0 \le \underline{p} \le \mathrm{Tr}\,[\mathbf{P}_k] \le \overline{p} < \infty$ for all k.*

3. *The rotation measurement errors $\tilde{\mathbf{R}}_{k+1}^k$ form a sequence of independent random matrices. The rotation and translation measurement errors $\tilde{\mathbf{R}}_j^{j-1}$ and $\tilde{\mathbf{t}}_{k-1,k}^k$ are mutually independent if $j \neq k$, and possibly dependent when $j = k$, with $\mathrm{E}[\tilde{\mathbf{R}}_k^{k-1}\ \tilde{\mathbf{t}}_{k-1,k}^k] =: \boldsymbol{\rho}_k \in \mathbb{R}^d$. There exists a scalar ρ such that $\|\boldsymbol{\rho}_k\| \le \rho$ for all k.*

4. *The relative translation measurement errors $\{\tilde{\mathbf{t}}_{k-1,k}^k\}_{k=1}^\infty$ are uniformly absolutely integrable, i.e., there exists a scalar β so that $\beta_k \le \beta < \infty$ for all k where $\beta_k := \mathrm{E}\,\|\tilde{\mathbf{t}}_{k-1,k}^k\|$.*

5. *The rotation measurement errors $\tilde{\mathbf{R}}_{k+1}^k$ are identically distributed, so that each $\tilde{\mathbf{R}}_{k+1}^k$ has the same distribution as that of some matrix $\tilde{\mathbf{R}} \in SO(d)$, $d \in \{2,3\}$. Moreover, $\tilde{\mathbf{R}}$ is not degenerate, i.e., its pdf (probability distribution function) is not concentrated on a set of measure zero.*

Apart from the assumptions on independence of measurement errors, the other assumptions, namely those on the existence of the parameters $\tau, b, \underline{p}, \overline{p}, \rho, \beta$, are trivially

satisfied in any practical scenario. Finiteness of the displacement τ and bias norm b are easy to see; the parameters $\underline{p}$ and $\overline{p}$ are simply the lower and upper bounds on the eigenvalues of $\mathbf{P}_k$. The d-dimensional vector $\boldsymbol{\rho}_k$ is a measure of the correlation between the translation and rotation measurements, and the parameter ρ is an upper bound on the magnitude of the correlation. We allow the relative translation and rotation measurement errors at a particular time instant to statistically dependent, since this may happen if there is overlap between the sensor suite used to obtain these two measurements. The parameter β is akin to an upper bound on the sum of bias and variance of the translation measurement error. To see this, consider not $\mathrm{E}[\|\tilde{\mathbf{t}}^k_{k-1,k}\|]$, but $\mathrm{E}[\|\tilde{\mathbf{t}}^k_{k-1,k}\|^2]$, which is the trace of the second moment of translation measurement error $\tilde{\mathbf{t}}^k_{k-1,k}$. Since the second moment is the sum of covariance and first moment, an upper bound on $\mathrm{E}[\|\tilde{\mathbf{t}}^k_{k-1,k}\|^2]$ is also an upper bound on sum of mean and variance (more precisely, on $\|\mathbf{b}_k\|^2 + \mathrm{Tr}\,[\mathbf{P}_k]$) of the translation measurement error.

The following technical result is crucial for the main results of this paper and will be required for the subsequent discussions. We therefore state it here; the proof is provided in the Appendix.

Proposition 1. *Let $\mathbf{R}$ be a random rotation matrix with distribution defined over $SO(d)$, $d \geq 2$ and let $\mathrm{E}[\mathbf{R}]$ be the $d \times d$ matrix whose i,j-th entry is the expected value of the i,-th entry of $\mathbf{R}$. We have $\|\,\mathrm{E}[\mathbf{R}]\| \leq 1$, and the inequality is strict if the distribution of $\mathbf{R}$ is not degenerate*[1]. □

Due to its usefulness in later discussions, we define

$$\overline{R} := \mathrm{E}[\tilde{\mathbf{R}}]. \tag{6}$$

Recall that $\tilde{\mathbf{R}}$ is a rotation matrix that has the same distribution as all the rotation errors $\tilde{\mathbf{R}}^k_{k+1}$, $k = 1, \ldots$. It follows from Proposition 1 that under Assumption 1,

$$1 > \gamma := \|\overline{R}\|. \tag{7}$$

According to the convention used in this paper, in general $\mathrm{E}[\mathbf{R}] \notin SO(d)$ even if $\mathbf{R} \in SO(d)$. It is important that the notation $\mathrm{E}[\mathbf{R}]$ is not to be understood as the expectation of the random variable $\mathbf{R}$ with a distribution defined over $SO(d)$, which we denote by $\mu_{\mathbf{R}}$, so that $\mu_{\mathbf{R}} \in SO(d)$. We call $\mu_{\mathbf{R}}$ the "Lie-group mean" of $\mathbf{R}$. We call an estimate $\hat{\mathbf{R}}$ of a true rotation R *unbiased* if $\mu_{\hat{\mathbf{R}}} = \mathbf{R}$. A result of the adopted convention is that for an unbiased estimator $\hat{\mathbf{R}}$ of $\mathbf{R}$, in general $\mathrm{E}[\hat{\mathbf{R}}] \neq \mathbf{R}$. The reason the quantity $\mathrm{E}[\mathbf{R}]$ is more useful for this paper than $\mu_{\mathbf{R}}$ is that when $\mathbf{R}$ and $\mathbf{t}$ are independent, $\mathrm{E}[\mathbf{R}\mathbf{t}] = \mathrm{E}[\mathbf{R}]\,\mathrm{E}[\mathbf{t}]$ but in general $\mathrm{E}[\mathbf{R}\mathbf{t}] \neq \mu_{\mathbf{R}}\,\mathrm{E}[\mathbf{t}]$. The bias in translation measurements obtained from vision-based sensors has been the subject of research [13, 12]. The bias in rotation measurement, on the other hand, seem to have drawn limited attention. In [12], the error in 3-D rotation is described in terms of the corresponding Euler angles, and bias in rotation is also defined in terms of the bias in the Euler angles. An alternate definition of 3-D rotation error in terms of a 3-vector (involving angle and axis of rotation) is used in [28], but the question of its bias is not discussed.

[1] Recall that we say the distribution of $\mathbf{R}$ is degenerate if its pdf is 0 everywhere except possibly in a set of measure 0.

3. Main results

3.1. General trajectories

Before stating the result, we recall the asymptotic O, Ω, Θ notation. For two scalar-valued functions $f(n), g(n)$ taking non-negative integer arguments, the notation $f(n) = O(g(n))$ means there exists a positive integer n_1 and a positive constant c_1 so that $f(n) \leq c_1 g(n)$ for all $n \geq n_1$. The notation $f(n) = \Omega(g(n))$ means there exists a positive integer n_2 and a positive constant c_2 so that $f(n) \geq c_2 g(n)$ for all $n \geq n_2$. The notation $f(n) = \Theta(g(n))$ means both $f(n) = \Omega(g(n))$ and $f(n) = O(g(n))$ hold.

Theorem 1. *Consider a robot moving in a 2-D or 3-D Euclidean space that performs position estimation from relative pose measurements as described in Section 2. Under Assumption 1, the following statements hold, where $\tau, \beta, b, \rho, \underline{p}, \overline{p}$ are parameters defined in Assumption 1 and γ is defined in* (7).

1. *The bias in the position estimation error satisfies $\|\,\mathrm{E}[\mathbf{e}(n)]\| = O(n)$. In particular,*

$$\max\left\{0, \|\mathbf{t}^0_{0,n}\| - \frac{1-\gamma^n}{1-\gamma}(\gamma\tau + \beta)\right\} \leq \|\,\mathrm{E}[\mathbf{e}(n)]\| \leq \|\mathbf{t}^0_{0,n}\| + \frac{1-\gamma^n}{1-\gamma}(\gamma\tau + \beta). \tag{8}$$

2. *The position error covariance satisfies $\mathrm{Tr}\,[Cov(\mathbf{e}(n), \mathbf{e}(n))] = O(n)$, with upper bound given by*

$$\mathrm{Tr}\,[Cov(\mathbf{e}(n), \mathbf{e}(n))] \leq \overline{\alpha_0}\left(\frac{1+\gamma}{1-\gamma}\, n\right), \tag{9}$$

where

$$\overline{\alpha_0} = \max\left\{(\tau^2 + 2\tau b + \overline{p} + b^2), (\tau + \frac{\beta}{\gamma})(\tau + b)\right\}. \tag{10}$$

If furthermore

$$\underline{p} \geq 2b\tau + \tau^2 + 2\frac{(\tau + \rho/\gamma)(\tau + b)}{1-\gamma}, \tag{11}$$

then

$$\mathrm{Tr}\,[Cov(\mathbf{e}(n), \mathbf{e}(n))] = \Theta(n). \qquad \square$$

Before discussing the implications of the theorem, we present a result in the form of a lemma that is useful in that discussion, as well as in the proof of the theorem. The proof of the lemma is provided in the Appendix.

Lemma 1. *Under Assumptions 1, the first and second moment of the position estimate satisfies*

$$\| \mathrm{E}[\hat{\mathbf{t}}^0_{0,n}]\| \leq \frac{1-\gamma^n}{1-\gamma}(\gamma\tau+\beta), \qquad \mathrm{E}[\|\hat{\mathbf{t}}^0_{0,n}\|^2] \leq \overline{\alpha_0}\frac{1+\gamma}{1-\gamma}\, n,$$

where $\overline{\alpha_0}$ *is defined in* (10)*. Moreover, if condition* (11) *is satisfied, then we have* $\mathrm{E}[\|\hat{\mathbf{t}}^0_{0,n}\|^2] = \Theta(n)$. □

3.2. Discussion on Theorem 1 and its proof

Theorem 1, and in particular the upper bound in (8), shows that if the robot's motion is confined to a bounded region, then the bias in the position estimation error stays uniformly bounded by a constant: $\| \mathrm{E}[\mathbf{e}(n)]\| = O(1)$. If the robot moves with a constant speed and with a constant (absolute) orientation, then its position grows linearly with time. In this case the theorem tells us that the bias grows linearly with time: $\| \mathrm{E}[\mathbf{e}(n)]\| = \Theta(n)$, since now both the upper and lower bounds are asymptotically linear in time. This implies that the asymptotic trend of the bias is crucially dependent on the robot's displacement.

This dependency of the bias on the robot's trajectory comes from the fact that that the estimated position is always bounded in mean, even if the robot is moving out to infinity, which follows from Lemma 1. To obtain an intuitive understanding of Lemma 1, we first note that the estimated position is simply the sum of the translations after transforming them to the common global coordinate frame 0; see (4). Taking expectation on both sides of (4), we obtain

$$\mathrm{E}[\hat{\mathbf{t}}^0_{0,n}] = \mathrm{E}[\hat{\mathbf{t}}^0_{0,1}] + \mathrm{E}[\hat{\mathbf{t}}^0_{1,2}] + \cdots + \mathrm{E}[\hat{\mathbf{t}}^0_{n-1,n}]. \tag{12}$$

The k^{th} term in the sum above, assuming rotation and translation measurements are independent, is

$$\begin{aligned}\mathrm{E}[\hat{\mathbf{t}}^0_{k-1,k}] &= \mathrm{E}\left[\left(\prod_0^{k-1}\hat{\mathbf{R}}^i_{i+1}\right)\hat{\mathbf{t}}^k_{k-1,k}\right] = \left(\prod_0^{k-1}\mathrm{E}[\hat{\mathbf{R}}^i_{i+1}]\right)\mathrm{E}[\hat{\mathbf{t}}^k_{k-1,k}] \\ &= \left(\prod_0^{k-1}\left(\mathbf{R}^i_{i+1}\overline{R}\right)\right)\mathrm{E}[\hat{\mathbf{t}}^k_{k-1,k}].\end{aligned}$$

The magnitude of this term is of order γ^k, since it involves k products of $\overline{R}$, each of which has a norm equal to γ. Since $\gamma < 1$ (see (7)), the sum (12) is bounded for all n. The expected value of the position estimate therefore converges to a point. Notice that the bounds (8) on the bias does not depend on the error in the translation measurements. The conclusions drawn above remain the same even if the rotation and translation measurements are unbiased, i.e., $\mu_{\tilde{\mathbf{R}}} = I$, $\mathbf{b}_k = 0$, and in fact, *even if the translation measurements are completely error free*, $\tilde{\mathbf{t}}^k_{k-1,k} = 0$.

The discussion above can be summarised into the following conclusions about the bias:

(i) For large time index n, the main contributions to the bias in the position estimate are the displacement of the robot and the errors in the relative rotation measurements.

(ii) The asymptotic scaling of the bias does not change even when the translation and rotation measurements are unbiased, and in fact even if translation measurements are completely error-free.

The first conclusion is well known, and is hardly surprising. However, conclusion (ii) does not seem to be recognized in the literature.

The variance growth rate does not seem to be sensitive to the trajectory of the robot. Furthermore, unlike the bias, the variance can grow without bound when the robot's trajectory is confined to a bounded region. We'll see evidence of this later in simulations and experiments reported in Sections 4 and 5. We believe that the sufficient condition (11) is conservative, and is an artifact of our proof technique. The condition (11) is usually not satisfied in practice since it requires a very large translation measurement error. Yet the position estimation error variance seems to be $\Theta(n)$ in simulations and experiments reported in Section 5.2.

The results of the theorem are in contrast to the prevalent belief in the literature that the error growth is superlinear in time if absolute orientation measurements are not available [4, 5, 6, 7, 8, 9, 10]. The theorem shows that even without absolute orientation sensors, localization error - or more precisely its bias and variance - grows at most linearly with time. We believe that the belief about superlinear growth came about from the fact that experiments/simulations were not conducted long enough to draw reasonable conclusion about asymptotic trends. Through the root cause is the geometric decay due to γ, since γ is usually quite close to 1, there is an initial period where the error grows sharply until the geometric decay kicks in and the linear trend becomes obvious. More insight into this phenomenon will be obtained later in Section 3.3 that discusses 2D trajectories (see in particular Theorem 2).

The proof of Theorem 1, presented next, follows from Lemma 1 in a straightforward manner.

Proof of Theorem 1. It follows from (5), by applying the triangle inequality that

$$\| \mathrm{E}[\mathbf{e}(n)]\| \leq \|\mathbf{t}^0_{0,n}\| + \| \mathrm{E}[\hat{\mathbf{t}}^0_{0,n}]\| \tag{13}$$

$$\| \mathrm{E}[\mathbf{e}(n)]\| \geq \max\left\{0, \|\mathbf{t}^0_{0,n}\| - \| \mathrm{E}[\hat{\mathbf{t}}^0_{0,n}]\|\right\} \tag{14}$$

From Lemma 1, we have that $\| \mathrm{E}[\hat{\mathbf{t}}^0_{0,n}]\|$ is upper bounded and so the first statement follows immediately from (13) and (14).

To prove the second statement, note that

$$\begin{aligned}\mathrm{Tr}\left[Cov(\mathbf{e}(n),\mathbf{e}(n))\right] &= \mathrm{Tr}\left[Cov(\hat{\mathbf{t}}^0_{0,n},\ \hat{\mathbf{t}}^0_{0,n})\right]\\ &= \mathrm{Tr}\left[\mathrm{E}[\hat{\mathbf{t}}^0_{0,n}(\hat{\mathbf{t}}^0_{0,n})^T] - \mathrm{E}[\hat{\mathbf{t}}^0_{0,n}]\,\mathrm{E}[\hat{\mathbf{t}}^0_{0,n}]^T\right]\\ &= \mathrm{E}[(\hat{\mathbf{t}}^0_{0,n})^T\hat{\mathbf{t}}^0_{0,n}] - \|\,\mathrm{E}[\hat{\mathbf{t}}^0_{0,n}]\|^2\\ &\le \mathrm{E}[(\hat{\mathbf{t}}^0_{0,n})^T\hat{\mathbf{t}}^0_{0,n}].\end{aligned}$$

Since $\|\,\mathrm{E}[\hat{\mathbf{t}}^0_{0,n}]\| = O(1)$, the second statement follows from Lemma 1. ■

3.3. Special 2-D trajectories

In this section we provide non-asymptotic results on the error growth for the special case when the motion of the robot is confined to a 2D plane and its trajectory is limited a certain type(s). In the 2-D scenario $\hat{\mathbf{t}}^i_{j,k}, \mathbf{t}^i_{j,k} \in \mathbb{R}^2$ and $\mathbf{R}^i_j, \hat{\mathbf{R}}^i_j \in SO(2)$ for every i, j, k. The x and y axes of a Cartesian coordinate frame that lies on this plane and is attached to the robot's body at the initial time $k = 0$ is used as the global coordinate frame. In the 2-D scenario, the robot's orientation at time n can be uniquely described by an angle $\theta_{0,n} \in [-\pi,\ \pi)$, which describes rotation of its local frame about the z-axis of the global frame. The relative rotation between the frames $k-1$ and k is uniquely determined by the angle by which the frame $k-1$ has to be rotated in the counter clockwise direction to reach frame k, which we denote by $\theta_{k-1,k}$. Figure 2 shows an example. A noisy measurement of the relative rotation, denoted by $\hat{\theta}_{k-1,k}$, is assumed available at time k. The error in the relative rotation measurement is

$$\tilde{\theta}_{k-1,k} := \hat{\theta}_{k-1,k} - \theta_{k-1,k}. \tag{16}$$

For future use, we define $f_R : [-\pi, \pi) \to SO(2)$ as

$$f_R(\alpha) := \begin{pmatrix}\cos\alpha & -\sin\alpha\\ \sin\alpha & \cos\alpha\end{pmatrix}.$$

The matrix $\mathbf{R}^{k-1}_k$ that describes the relative rotation between the frames $k-1$ and k is therefore given by $\mathbf{R}^{k-1}_k = f_R(\theta_{k-1,k})$. It can be shown from the definition (1) that

$$\tilde{\mathbf{R}}^{k-1}_k = f_R(\tilde{\theta}_{k-1,k}). \tag{17}$$

The estimate of the rotation $\mathbf{R}^{k-1}_k$ therefore is $\hat{\mathbf{R}}^{k-1}_k = f_R(\hat{\theta}_{k-1,k})$.

The first result, which is stated below, is on the position estimation error growth rate when the robot moves in a straight line with constant velocity and orientation. The proof of the theorem is in the Appendix.

Theorem 2. *Consider a robot that moves on a 2-D plane in a straight line with a constant orientation. Formally, for all k, $\theta_{k-1,k} = 0$ and $\mathbf{t}^k_{k-1,k} = \mathbf{r} \in \mathbb{R}^2$, for some vector $\mathbf{r}$. In addition to Assumption 1, assume that the relative orientation error $\tilde{\theta}$ has a pdf that is symmetric around its mean $\mathrm{E}[\tilde{\theta}]$, the translation measurement errors $\tilde{\mathbf{t}}^k_{k-1,k}, k = 1, \ldots$ are wide sense stationary with $\mathbf{b}_k = \mathbf{b}$, $\mathbf{P}_k = \mathbf{P}$, and $\boldsymbol{\rho}_k = \boldsymbol{\rho}$ for all k. In that case, we have*

$$\begin{aligned}&\mathrm{E}[\mathbf{e}(n)] = n\,\mathbf{r} - (I - c\underline{\mathbf{R}})^{-1}\,(I - (c\underline{\mathbf{R}})^n)\,(c\underline{\mathbf{R}}\mathbf{r} + \boldsymbol{\rho}),\\ &\mathrm{Tr}\left[Cov(\mathbf{e}(n),\mathbf{e}(n))\right] = \psi n + \omega(n),\end{aligned} \tag{18}$$

where

$$c := \mathrm{E}[\cos\left(\tilde{\theta} - \mathrm{E}[\tilde{\theta}]\right)], \qquad \underline{\mathbf{R}} := f_R(\mathrm{E}[\tilde{\theta}]), \tag{19}$$

and the scalars ψ, $\omega(n)$ are given in (15). □

Since the r.v. $\tilde{\theta}$ is not degenerate by Assumption 1, we have that $|c| < 1$. The spectral radius of $c\underline{\mathbf{R}}$ is strictly lower than unity since $|c| < 1$ and $\underline{\mathbf{R}} \in SO(2)$. Hence $I - c\underline{\mathbf{R}}$ is invertible and $\psi, \omega(n)$ in (15) are well defined.

An immediate corollary of Theorem 2 is that for straight line motion, both the bias and the variance of the position estimation error grow asymptotically linearly with time. This follows from the expressions for the bias and the variance upon using the fact that $c < 1$. However, due to the presence of the c^n terms, the growth looks superlinear for intermediate values of the time index n. Simulations described in Section 4.2 verify this statement; see in particular Figure 5 and 6. The linear trend becomes visible only when large values of the time index n are considered. This may be one of the reasons that the error is believed to grow super-linearly with time in the literature.

The next case is a periodic trajectory in 2-D. We say the robot moves in a *periodic trajectory with period p* if the absolute orientation and position of the robot satisfies the following conditions: $\theta_{0,k} = \theta_{0,k+p}$ and $\mathbf{t}^0_{0,k} = \mathbf{t}^0_{0,k+p}$ for all k. The shape of the (closed) path along which the robot moves can be arbitrary. In the statement of the theorem, η denotes the number of periods up to time n, and q to denote the residual, i.e., $\eta(n) := \lfloor n/p \rfloor$ and $q := n - \eta p$.

Theorem 3. *Consider a robot moving in $\mathbb{R}^2$ whose trajectory is periodic with period p. In addition to Assumption 1.1-Assumption 1.4, assume that the first and second moments of the measurement errors are periodic with period p (so that $\mathbf{b}_k = \mathbf{b}_{k+p}$, $\boldsymbol{\rho}_k = \boldsymbol{\rho}_{k+p}$ and $\mathbf{P}_k = \mathbf{P}_{k+p}$). In that case,*

$$\begin{aligned}\mathrm{E}[\mathbf{e}(n)] = \mathbf{t}^0_{0,q} &- (I - (c\underline{\mathbf{R}})^p)^{-1}\\ &\times (I - (c\underline{\mathbf{R}})^{\eta p})\,w(p) - (c\underline{\mathbf{R}})^{\eta p} w(q),\end{aligned} \tag{20}$$

where $w(j)$ is given by

$$w(j) := \sum_{i=0}^{j-1} (c\underline{\mathbf{R}})^i\,\mathbf{R}^0_{i+1}\left(c\underline{\mathbf{R}}\,\mathbf{t}^{i+1}_{i,i+1} + \boldsymbol{\rho}_i\right),$$

where $c, \underline{\mathbf{R}}$ are as defined in Theorem 2.

$$\psi = 2c\mathbf{r}^T \left(I - c\underline{\mathbf{R}}\right)^{-1} \underline{\mathbf{R}}\mathbf{r} + \mathrm{Tr}\left[\mathbf{P} + \mathbf{b}\mathbf{b}^T\right] + (2\mathbf{b}^T + \mathbf{r}^T)(I - c\underline{\mathbf{R}})^{-1}\boldsymbol{\rho} \tag{15}$$

$$\begin{aligned}\omega(n) = {} & \mathbf{r}^T(I - c\underline{\mathbf{R}})^{-2}\left(I - 4c\underline{\mathbf{R}} + 2(c\underline{\mathbf{R}})^2 + 2(c\underline{\mathbf{R}})^{n+1}\right)\mathbf{r} - 2\mathbf{b}^T(I - c\underline{\mathbf{R}})^{-2}\left(I - (c\underline{\mathbf{R}})^n\right)\boldsymbol{\rho} \\ & + \mathbf{b}^T(I - c\underline{\mathbf{R}})^{-1}\left[I - (c\underline{\mathbf{R}})^n\right]\mathbf{r} - \mathbf{r}^T(I - c\underline{\mathbf{R}})^{-2}\left[I - (c\underline{\mathbf{R}})^n\right]\boldsymbol{\rho} - \| \left[(I - c\underline{\mathbf{R}})^{-1}(I - (c\underline{\mathbf{R}})^n)(c\underline{\mathbf{R}}\mathbf{r} + \boldsymbol{\rho})\right] \|_2^2\end{aligned}$$

The proof of the theorem is provided in the Appendix. The assumption of the moments $\boldsymbol{\rho}_k$ etc. being periodic with period p is motivated by the use of vision-based sensors to measure relative poses. In that case the measurement error statistics may depend on the scene the camera sees, which will repeat itself every p instants due to the periodic nature of the robot's motion. Note that i.i.d. errors are a special case of errors with periodic statistics, so the result also holds if all the measurement errors are i.i.d.

It can be shown in a straightforward manner from (20) that the bias is $O(1)$, by using the fact that $|c| < 1$. This is consistent with Theorem 1 since the robot stays in a bounded region for all time when following a periodic trajectory.

4. Simulation verification

In this section we empirically estimate the mean and covariance of the estimation error by conducting Monte-Carlo simulations and compare them with the theoretical predictions. In section 4.1 we simulate a robot moving along a randomly generated 3-D path and compare the results with the upper and lower bounds predicted in Theorem 1. In sections 4.2 and 4.3 we present simulations for the 2-D scenario with straight line and periodic trajectories so that empirical results can be compared with predictions of Theorem 2 and 3. Here the robot is simulated moving along either the straight line or periodic trajectory at a speed of 0.32 m/s for about 5.5 hours, traveling a distance of 6400 meters. In all three simulations, measurements of the robot's relative pose were taken every 0.2 seconds. All simulations are conducted in MATLAB©. To the extent possible, the parameters used in the simulations are the same as those in the experiments.

4.1. 3-D Simulation

For the 3-D case we simulate a robot moving along a path that is shown in Figure 3. The robot traverses this path from the starting point to the left and moving to the right. Measurement errors are generated as follows. The error in rotation ($\tilde{\mathbf{R}}_k^{k-1}$) is introduced by applying a random unit-quaternion at each time step drawn independently from a Von Mises-Fisher distribution with concentration parameter $k = 10000$. The reader is referred to [29] for details on Von Mises-Fisher distribution. The errors in relative translation at each time step ($\tilde{\mathbf{t}}_{k-1,k}^k$) are drawn from a zero-mean normal random variable with covariance matrix $(2.5\times10^{-5})\, I_{3\times3}$. The corresponding constants necessary to compute the upper bounds in Theorem 1 are obtained from randomly generated measurements to simulate a sensor characterization test and found to be $\gamma = 0.9997$, $\tau = 0.1295$ m, $\mathrm{b} = 0$ m, $\beta = 0.008$ m, $\underline{\mathrm{p}} = 7.45 \times 10^{-5}$ m^2, and $\overline{\mathrm{p}} = 7.55 \times 10^{-5}$ m^2

Figure 4 compares the empirically estimated bias and variance with the upper bounds given by Theorem 1. The empirical estimates are obtained from 4500 Monte Carlo simulations. As predicted by the theorem, the bias in the position estimate grows without bound since the robot's position is growing (in norm) without bound. We see that the bounds predicted by the theorem are of the same order of magnitude as values obtained empirically. However, the bounds for the variance are rather loose.

4.2. Straight-line 2-D trajectory

For the straight line case, we simulate a robot moving in a straight line on a plane with a constant velocity of $[0.2263, 0.2263]^{\mathrm{T}}$ m/s and constant orientation. Two types of simulations are conducted.

In the first type, which we call *simulated data*, noisy measurements of the rotation, i.e., $\hat{\theta}_{k-1,k}$ are generated as a Laplace distributed random variable using a pseudo-random number generator. The reason for choosing a Laplace distribution, over, say a Gaussian, is the following. We obtained a large sample of 2D orientation estimates from images taken with a machine-vision camera and performed hypothesis testing for three distributions: Laplacian, Gaussian and Fisher Von-Mises. Only the Laplace distribution passed the test. We refrain from giving details of the hypothesis testing here; they can be obtained from the authors upon request. Noisy measurements of the translations, i.e., $\hat{\mathbf{t}}_{k-1,k}^k$ were generated from noisy measurements of translation direction, which we call $\boldsymbol{\zeta}_{k-1,k}^k$, and translation magnitude, which we call $d_k \in \mathbb{R}^+$, as $\hat{\mathbf{t}}_{k-1,k}^k = \hat{d}_k \hat{\boldsymbol{\zeta}}_{k-1,k}^k$, where $\hat{d}_k$ and $\hat{\boldsymbol{\zeta}}_{k-1,k}^k$ are noisy estimates of d_k and $\boldsymbol{\zeta}_{k-1,k}^k$, respectively. Note that $\boldsymbol{\zeta}_{k-1,k}^k$ is a 2-vector with unit norm. This is done to simulate relative pose measurement with IMU/wheel odometry and a monocular camera without scale information. The camera provides relative translation direction but not the magnitude of translation, which is measured by IMUs/wheel encoders.

In the second type of simulations, which we call by *simulated camera*, the vision-based relative pose estimation sensor is simulated in a more realistic fashion by generating synthetic image data, from which relative rotation

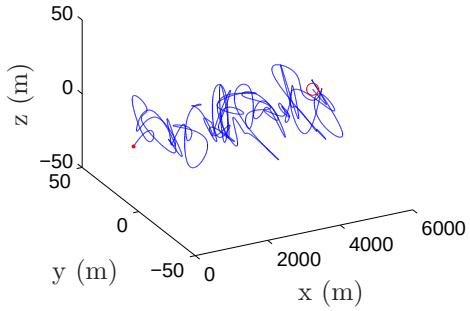

Figure 3: The 3-D path used for the simulation in section 4.1. The red dot indicates the robots initial location, while the red circle indicates the robots final location.

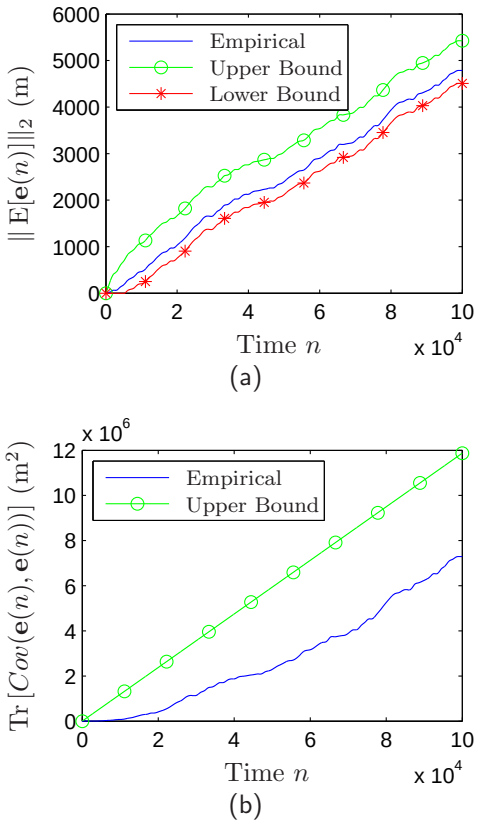

Figure 4: 3-D scenario: Comparison of Theorem 1's predictions ("Upper Bound" and "Lower Bound") of bounds on the bias and variance in position estimation error with those estimated from Monte-Carlo simulations ("Empirical").

and direction of translation are estimated. The magnitude of translation measurements are generated as in the "simulated data" case.

Simulated data: At each time step k, a measurement of the relative orientation is constructed numerically as $\hat{\theta}_{k-1,k} = 0 + \tilde{\theta}_{k-1,k}$, where the orientation error $\tilde{\theta}_{k-1,k}$ is chosen to be a 0-mean Laplace distributed r.v. Recall that a Laplace distribution with μ mean and variance $2\lambda^2$ has the pdf $f(\tilde{\theta}) = \frac{1}{2\lambda} e^{-|\tilde{\theta}-\mu|/\lambda}$. The value of λ chosen is 3.6×10^{-3}, which best fits the orientation measurement error statistics generated by the synthetic monocular camera-based relative pose sensor that is used in the experiments described in the sequel. The noisy measurement of translation direction $\hat{\boldsymbol{\zeta}}^k_{k-1,k}$ generated as

$$\hat{\boldsymbol{\zeta}}^k_{k-1,k} = \begin{pmatrix} \cos\tilde{\phi}_{k-1,k} & -\sin\tilde{\phi}_{k-1,k} \\ \sin\tilde{\phi}_{k-1,k} & \cos\tilde{\phi}_{k-1,k} \end{pmatrix} \boldsymbol{\zeta}^k_{k-1,k}$$

where $\tilde{\phi}_{k-1,k}$ is a zero-mean Laplace random variable with variance 3.07×10^{-2} rad^2 , and $\boldsymbol{\zeta}^k_{k-1,k} = \frac{1}{\sqrt{2}}[1,1]^T$ is the true translation direction. The magnitude of the translation is $d_k = 6.4 \times 10^{-2}$ m and its noisy measurement is generated as $\hat{d}_k = d_k + \tilde{d}_k$, where $\tilde{d}_k$ is a zero-mean Gaussian random variable with mean 0 variance 8.5467×10^{-5} m^2. These numbers are chosen to be consistent with those seen in an experiment with a wheeled robot described later in Section 5. The parameters $\mathbf{b}, c, \mathbf{P}, \boldsymbol{\rho}$ that are needed to compute the predictions by Theorem 2, are estimated by a simulated sensor characterization test, i.e., by appropriate averaging of randomly generated data. They turn out to be $\mathbf{b} = [-0.6842, -0.6842] \times 10^{-3}$ m, $c = 1 - 1.2873 \times 10^{-5}$, $\mathrm{Tr}\,[\mathbf{P}] = 1.2479 \times 10^{-4}$ m^2, and $\boldsymbol{\rho} = c\mathbf{b}$.

The mean and covariance of the position estimation error at every time instant are empirically estimated by averaging over 76,600 Monte-Carlo simulations. Figure 5 presents the estimated mean and covariances, and the values predicted by Theorem 2. We see from the figure that the prediction from Theorem 2 matches estimates from Monte-Carlo simulations quite closely even for the large time intervals used in the simulations.

Simulated camera: We now simulate the scenario in which relative pose measurements are obtained by a calibrated monocular Prosilica EC 1020 camera and wheel odometers found on a Pioneer P3-DX. To simulate an estimate of the camera ego-motion between consecutive time steps, suppose between k and $k+1$, a set of 50 3-D points are randomly generated in the volume visible to the camera at time step k, with their coordinates represented in the coordinate frame attached to the camera at time step k. The points are then acted on by the true transformation from k to $k+1$ to find the corresponding coordinates in the coordinate frame attached to the camera at time step $k+1$, discarding any points falling outside the volume visible to the camera at that time step. Using a calibration matrix corresponding to the Prosilica EC 1020 camera, the points are projected into their corresponding image plane. This forms a set of correspondences analogous to the feature points extracted from actual image pairs. Each feature point is now corrupted by uniform noise with support lying in a 2×2 pixel square about the point. A RANSAC [30] assisted normalized 8-point algorithm [31] is used to estimate the rotation $\hat{R}$ and translation direction $\hat{\boldsymbol{\zeta}}$ between the two time steps from these point correspondences. The axis of rotation was then aligned with the normal to the plane of motion and the component of the translation vector in that direction was dropped to insure the

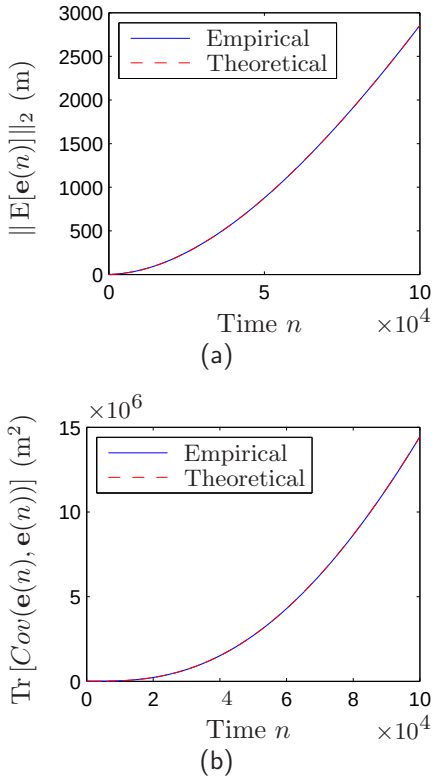

Figure 5: 2-D scenario, straight line trajectory: Comparison of Theorem 2's predictions ("Theoretical") of bias and variance in position estimation error with those obtained from Monte-Carlo simulations ("Empirical"), for the "simulated data" case.

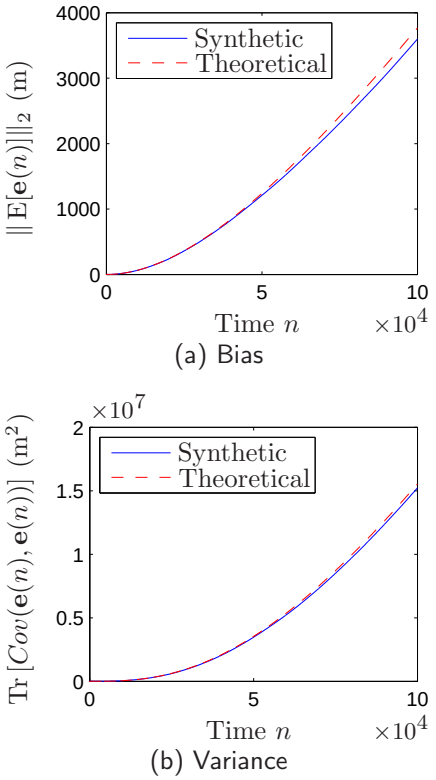

Figure 6: 2-D scenario, straight line trajectory: Comparison of Theorem 2's predictions ("Theoretical") of bias and variance in position estimation error with those obtained from Monte-Carlo simulations ("Synthetic"), for the "simulated camera" case.

motion estimates remained in the plane. The magnitude of translation $\hat{d}$ is generated as in the **Simulated Data** case. The values of the parameters that are needed to compute the predictions by Theorem 2 are estimated from a simulated sensor characterization test like before. The values are found to be $\mathbf{b} = [-0.5767, -0.5904] \times 10^{-5}$ m, $\mathrm{Tr}\,[\mathrm{P}] = 1.6382 \times 10^{-4}\,\mathrm{m}^2$, and $c = 1 - 2.1462 \times 10^{-5}$.

Figure 6 compares the predictions of bias and variance by Theorem 2 to those estimated from 1000 Monte-Carlo simulations. The number of Monte-Carlo simulations is smaller in the synthetic data case due to the prohibitively high cost of conducting these simulations. We see from Figure 6 that Theorem 2 accurately predicts the position estimation error computed from synthetic image data. The prediction toward the end of the simulation time is not as accurate as in the simulated data case, which is due to the smaller number of Monte-Carlo trials.

4.3. Periodic trajectory

We now simulate a robot moving on a circle with circumference of 4.11 m so that its trajectory is periodic with period $p = 3020$. The speed of the robot is approximately 0.32 m/s, so that it traverses the circle about 47 times before completing one period. The trajectory is chosen to be close to that encountered in an experiments with a Pioneer P3-DX robot, which will be described in Section 5. Noisy relative pose measurements are generated as in the **Simulated Data** case in straight line motion. Orientation measurement errors are Laplace distributed (with mean $\mathrm{E}[\tilde{\theta}] = 6.8 \times 10^{-5}$ m and parameter $\lambda = 3.6 \times 10^{-3}$) while translation measurement errors are generated in the same manner, and with the same distributions as in the **Simulated Data** case in straight line motion; with the new true values given by $\boldsymbol{\zeta}_{k-1,k}^{k} = -[0.049, 0.999]^T$ and $\mathrm{d_k} = 0.064$ m.

Figure 7 shows the empirical estimates of bias and variance from 29,970 Monte-Carlo simulations. It also presents the bias predicted from Theorem 3. We see from Figure 7(a) that the bias is quite accurately predicted by Theorem 3. The high frequency oscillation corresponds to the time it takes for the robot to traverse the circle once. The lower frequency oscillation corresponds to the period of the trajectory. The variance seems to grow linearly with time, as one can see from Figure 7(b), but a formula is not available in the periodic case for comparison.

5. Experimental verification

In this section we report results of experiments conducted with a wheeled Pioneer P3-DX robot that is equipped with a calibrated monocular Prosilica EC 1020

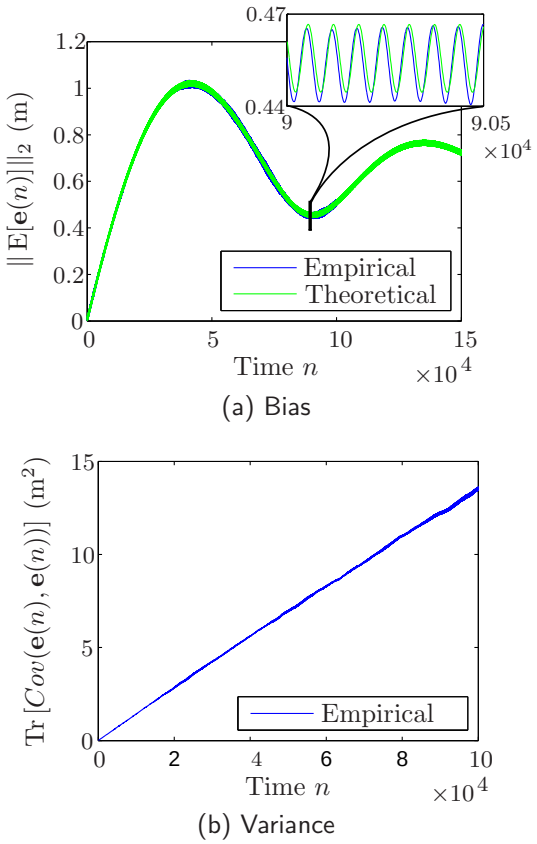

Figure 7: 2-D scenario, periodic motion: Comparison of Theorem 3's predictions with estimates from Monte-Carlo simulations ("Empirical"). The legend "Theoretical" in (a) refers to the prediction from (20) in Theorem 3.

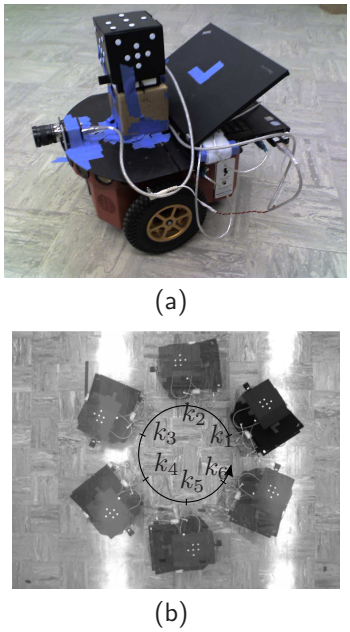

Figure 8: (a)The robot used in the experiments, and (b) a few snapshots from the overhead camera showing the trajectory.

camera and wheel odometers. The images captured by the camera are used to estimate the relative rotation and direction of translation. The distance travelled estimated by the wheel odometers is fused with the direction of translation estimated from the camera to estimate the translation vector. The relative pose of the camera is measured every 0.2 seconds. An overhead camera is used to measure the true 2-D pose of the robot. Due to space constraints of the indoor test set-up, the trajectory of the robot was chosen to be an approximately circular one with radius 0.65 m and one rotation taking approximately 13 seconds (see Figure 8). Although the robot's trajectory is not truly periodic; it is approximately periodic with period $p = 3020$ (i.e., 604 seconds).

5.1. Test set-up

Figure 9(b) shows a schematic of the experimental set-up. The global coordinate frame is defined to coincide with the coordinate frame attached to an overhead camera viewing the plane of motion. That is, the origin of the global coordinate axes corresponds to the camera's focal point. The overhead camera is used to obtain the true pose of the robot. The robot's local coordinate frame was defined by a cube affixed to the top of the box. A grid consisting of six dots was placed atop the cube with a known geometry (see Figure 9(a)), which allows reconstruction of the full 3-D pose of the robot from the single monocular camera. Although some error between the true pose of the robot and that estimated from the overhead camera is inevitable, this error did not have any cumulative effect over time. Therefore the pose estimated from the overhead camera is taken as the ground truth.

A KLT tracker [32] was used to track feature points across pairs of images, and a RANSAC-assisted normalized 8-point algorithm was used to estimate the relative rotation and direction of translation between every successive pairs of images. All estimation was performed off-line. Even with RANSAC, outliers in point-correspondences can cause large errors in the relative pose estimates. An ad-hoc "filter" was implemented to reduce the effect of such errors as follows. If the estimated relative pose from the camera was deemed infeasible (which was determined by the known motion of the robot), the relative rotation and relative translation direction estimated in the previous time step was used as the estimate for the current time step. The relative translation between two time instants was estimated from the relative translation direction and the estimate of its magnitude, the latter being obtained from a wheel odometer. The relative poses so obtained were chained together to obtain an estimate of the global position and orientation of the robot at every time step, as described in Section 2.

5.2. Test results

The position estimation error at each time step is computed by comparing the ground truth with the robot's position estimated from relative pose measurements. The bias and variance in the position estimation error at any

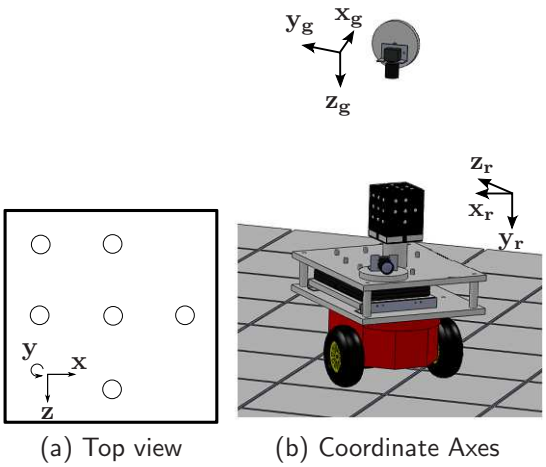

Figure 9: Schematic of the test set-up.

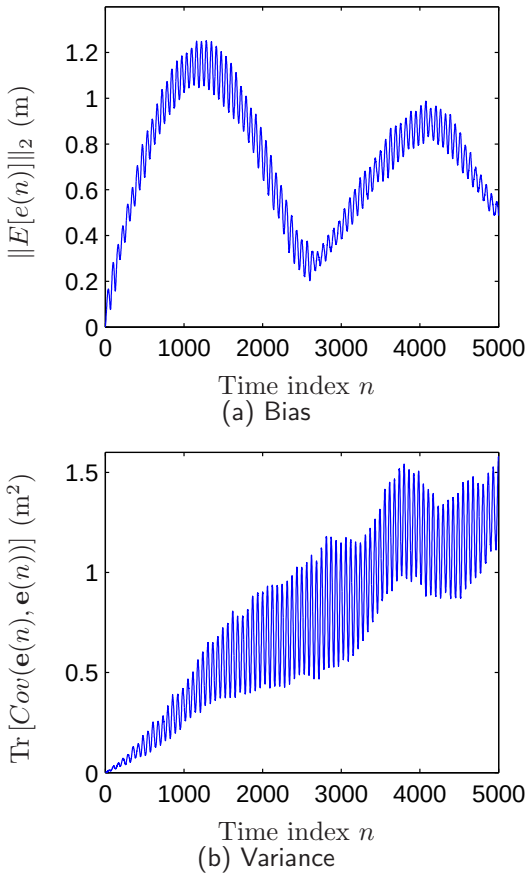

Figure 10: Experimental results: bias and variance of position estimation error for a P3-DX robot (5000 time steps = 16.67 minutes).

given time step are determined by averaging over 17 experiments, where each experiment consists of the robot moving on its path for 1000 seconds (5000 time steps). The experimentally obtained bias and variance of position estimation error are shown in Figures 10(a) and 10(b).

We see from the figures that the experimentally obtained results - especially the bias – closely resemble those seen in simulations (cf. Figure 7(a),7(b)), which in turn are accurately predicted from the analysis. The experimentally obtained bias stays bounded, as Theorem 3 predicts. The variance also shows an on-average linear growth with time, which is consistent with Theorem 1. The experiment provides additional confidence in our theoretical results. In addition, we note that while the theoretical predictions are for a dead-reckoning type position estimation algorithm, the algorithm used in the experiments was more akin to a kinematic-model based filter. Still the theoretical predictions match the experimental results rather well. This is expected since - as argued earlier - the analysis is applicable to broader class of estimation algorithms; see the discussion in Section 2 after Eq. (5).

There are nevertheless some discrepancies between the experimentally obtained bias and variance values and those obtained from simulations, as can be seen comparing Figure 7(a) with Figure 10(a) and Figure 7(b) with Figure 10(b). These are due to the differences between the experiments and simulations. First, the experimental bias and variances values are computed by averaging over *only 17* experiments, whereas the simulation estimates are computed from at least 1000 Monte-Carlo simulations, in some cases many more. The reason for this smaller number of experimental trials is the difficulty and time needed in performing these experiments. The smaller number of trials that were averaged over produced less accurate estimates. Second, the characteristics of the camera error could not be modeled in any of our simulations. Third, it is not possible to ensure a truly periodic trajectory in a real experiment. The "high-frequency" oscillations in the experimental bias and variance plots are at 7.8×10^{-2} Hz, which correspond to the average time the robot takes to traverse the circle once. These are seen in the simulations as well; see in particular the inset in Figure 7(a). However, these oscillations are not particularly visible in the variance, one has to magnify the curve in Figure 7(b) considerably to see them. We believe the noticeable difference in case of the variance comes from the very small number of runs that we averaged over.

6. Reducing the bias

We now discuss a possible way to reduce the bias in the position estimate by using the lessons learned from the analysis that led to Theorem 1. First of all we note that computing $\mathrm{E}[\hat{\mathbf{t}}^0_{k-1,k}]$ requires knowledge of true relative rotations and translations, and therefore the bias cannot be eliminated by simply computing it and subtracting it from the estimated translation $\hat{\mathbf{t}}^0_{k-1,k}$ at every k. Instead the proposed method consist of modifying the *raw* measurements $\hat{\mathbf{R}}_k^{k-1}, \hat{\mathbf{t}}^k_{k-1,k}$ into the so-called *modified* measurements $(\hat{\mathbf{R}}_k^{k-1})_{modif}, (\hat{\mathbf{t}}^k_{k-1,k})_{modif}$, that are defined below, and then using them in the position estimation.

$$(\hat{\mathbf{R}}_k^{k-1})_{modif} := \hat{\mathbf{R}}_k^{k-1}(\overline{R})^{-1} \qquad (\hat{\mathbf{t}}^k_{k-1,k})_{modif} := \hat{\mathbf{t}}^k_{k-1,k} - \mathbf{b},$$

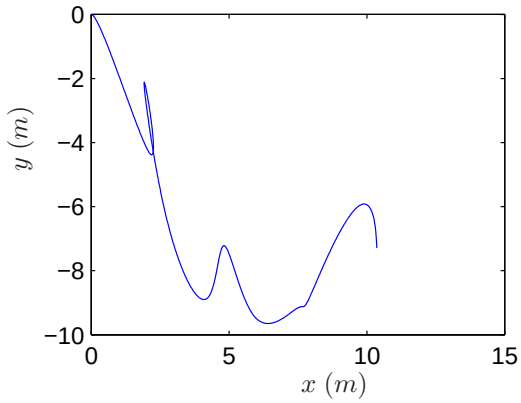

Figure 11: A randomly generated path in 2D used to test the bias-reduction method.

where

$$\mathbf{b} := \mathrm{E}[\tilde{\mathbf{t}}^k_{k-1,k}], \quad k \geq 1. \tag{21}$$

We are assuming that the translation measurements are stationary in mean so that $\mathbf{b}$ is a constant. The modified measurements can be computed from the raw measurements and knowledge of $\overline{R}, \mathbf{b}$, which can be determined from an analysis of sensor noise characteristic. For instance, the question of estimating $\mathbf{b}$ for vision-based sensors is examined in [13, 12]. The position at time k is now computed as before, but with the new corrected measurements in place of the raw sensor measurements $\hat{\mathbf{t}}^k_{k-1,k}$ and $\hat{\mathbf{R}}^{k-1}_k$. Specifically,

$$(\hat{\mathbf{R}}^0_k)_{modif} := \prod_{i=1}^{k} (\hat{\mathbf{R}}^{i-1}_i)_{modif}$$

$$(\hat{\mathbf{t}}^0_{k-1,k})_{modif} := (\hat{\mathbf{R}}^0_k)_{modif}\,(\hat{\mathbf{t}}^k_{k-1,k})_{modif},$$

$$\text{and finally, } (\hat{\mathbf{t}}^0_{0,n})_{modif} = \sum_{k=1}^{n} (\hat{\mathbf{t}}^0_{k-1,k})_{modif}.$$

The rationale for this proposal comes from the following relationships that can be shown from straightforward calculations:

$$\mathrm{E}[(\hat{\mathbf{R}}^{k-1}_k)_{modif}] = \mathbf{R}^{k-1}_k \tag{22}$$

$$\mathrm{E}[(\hat{\mathbf{R}}^{k-1}_k)_{modif}(\hat{\mathbf{t}}^k_{k-1,k})_{modif}] = \mathbf{R}^{k-1}_k \mathbf{t}^k_{k-1,k}, \tag{23}$$

where the second relation (23) holds if the raw rotation and translation measurements $\hat{\mathbf{R}}^{k-1}_k$, $\hat{\mathbf{t}}^k_{k-1,k}$ are uncorrelated. The modification of the raw measurements eliminates the geometric decay of the length of the relative translation measurements after being transformed to frame 0. As discussed in Section 3.2, this decay was the main cause of the bias growth. If $\hat{\mathbf{R}}^{k-1}_k$, $\hat{\mathbf{t}}^k_{k-1,k}$ are correlated but the motion is limited to a 2-D space, a slightly different method can be used that ensures that (22),(23) hold. The details are not provided in the interest of space.

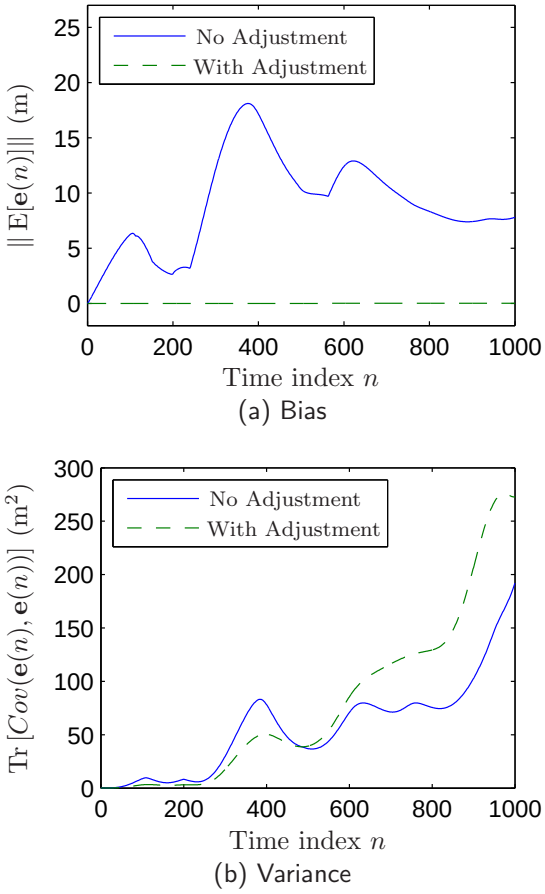

Figure 12: Performance of the bias-reduction method, for the path shown in Figure 11. The legend "With Adjustment" refers to the estimates obtained with the bias-reduction method of Section 6. The bias is reduced to almost zero with the proposed method. All quantities are estimated from more than a million Monte-Carlo simulations.

The proposed method was tested with the help of simulations to determine its effectiveness. The following types of trajectories in 2-D were used in the simulations: (i) straight line (ii) circular, (iii) random walk in a city-like grid, and (iv) a randomly generated smooth path. The performance was seen to be similar in all cases; so we only present the details for the last case. The path our robot traversed in the experiment is shown in Figure 11. Noise in the sensor measurements was simulated by adding i.i.d. Gaussian random vectors with mean $[0.05, 0.02]^T$ m and covariance matrix $0.05I$ to the relative translation measurements at each time step. The angle describing the relative rotation between each time step was corrupted by adding i.i.d. Gaussian random variables with mean 6.8×10^{-3} and variance 2.6×10^{-3}. The sensor characteristics $\overline{R}$ and $\mathbf{b}$ needed for the correction were determined a-priori; their values are $\overline{R} = 0.9987 f_R(6.8 \times 10^{-3})$, $\mathbf{b} = [0.05, 0.02]^T$. The estimates of the bias and variance in the position estimates were obtained from more than a million Monte-Carlo simulations. The comparison between the bias with the method described in Section 6

and that for the baseline case (no modification) is shown in Figure 12(a). The comparison of the variances is shown in Figure 12(b).

We see from the simulations that the proposed method significantly reduces the bias. The resulting variance is the same or smaller, for *small values of time*. For large values of time, the resulting variance is larger than that achieved if measurements were not modified. This is expected since the modifications introduce additional uncertainty. In particular, the modified rotation measurements are no longer elements of $SO(d)$. A similar trend is seen for all other trajectories tested: the bias is significantly reduced for all time, while the variance is either smaller or almost the same for small values of time but is larger for large values time.

7. Summary

We examined the growth of error in position estimates obtained from noisy relative pose measurements. We showed that in both 2-D and 3-D, the bias and the variance of the position estimation error grows at most linearly with time or distance travelled. The precise growth rate of the bias depends on the trajectory of the robot. Specifically, if the robot stays in a bounded region, the bias is upper bounded by a constant for all time. It was proved that the variance growth rate is also lower bounded by linear function of time if the translation measurement errors are large enough. Exact formulas for the error bias and variance were obtained for two special 2-D trajectories, straight line and periodic. Extensive Monte-Carlo simulations, and experiments with a wheeled robot, were used to verify the results.

The results of this paper show that localization error growth rate is not superlinear with time or distance even without absolute orientation sensors. In addition, it turns out that the asymptotic growth rate of the bias does not change even if all the measurements are unbiased or even if the translation measurements are completely error free. The bias growth is principally due to the fact that the expected value of the estimated position converges to a point, irrespective of how the robot is moving. This occurs since γ, the norm of the expected rotation error, is strictly less than unity. As a result, the magnitude of the measured translation, once the measurement is transformed to the global coordinate frame, decays geometrically with time.

One of the assumptions made for the analysis was that the measurements collected at two distinct time instants are statistically independent. Though this may not hold in practice, the results obtained from experiments and simulations with synthetic image data are consistent with the theoretical predictions. This shows that the analysis is not sensitive to the the assumptions of independence. The sufficient condition (11) for the variance to be asymptotically linear in time is not satisfied in the simulations and the experiment. However, the empirically estimated variance from simulations and experiment seems to grow linearly with time. This indicates that the sufficient condition is conservative. Determining a necessary condition for variance growth to be linear is an open question.

A method to reduce the bias growth rate was suggested by the lessons learned in the analysis of error growth. Simulations showed that the proposed method reduces the bias significantly for all time, while having negligible effect on the variance for small values of time. Thus the method can be potentially used to improve localization accuracy for short periods of time. There are several issues that still need to be addressed. The method was observed to make the variance worse for large time. So an important research question is to determine the time period up to which the method can be used. The method requires knowledge of sensor characteristics. Its robustness to imprecise knowledge of sensor characteristics, and to time variations in those characteristics, also needs to be studied. Another line of research is to incorporate the proposed bias reduction method within a filtering-type position estimation algorithm.

8. Acknowledgment

The research reported in this paper is based upon work supported by the Institute for Collaborative Biotechnologies through grant W911NF-09-D-001 “GeoTrack: Target Localization and Tracking by Networked Unmanned Systems” from the U.S. Army Research Office. The authors acknowledge the University of Florida High-Performance Computing Center for providing computational resources and support that have contributed to the research results reported within this paper.

References

[1] T. Oskiper, Z. Zhu, S. Samarasekera, R. Kumar, Visual odometry system using multiple stereo cameras and inertial measurement unit, in: IEEE Conference on Computer Vision and Pattern Recognition (CVPR ’07), 17-22 June 2007, pp. 1–8. doi:10.1109/CVPR.2007.383087.

[2] O. Mezentsev, G. Lachapelle, Pedestrian dead reckoning - a solution to navigation in GPS signal degraded areas?, Geomatica 59 (2) (2005) 175–182.

[3] R. C. Smith, P. Cheeseman, On the representation and estimation of spatial uncertainty, International Journal of Robotics Research 5 (4) (1986) 56–68.

[4] C. F. Olson, L. H. Matthies, M. Schoppers, M. W. Maimone, Rover navigation using stereo ego-motion, Robotics and Autonomous Systems 43 (4) (2003) 215–229.

[5] H. Badino, A robust approach for ego-motion estimation using a mobile stereo platform, in: International Workshop on Complex Motion, 2004, pp. 198–208.

[6] M. Klopschitz, D. Schmalstieg, Automatic reconstruction of wide-area fiducial marker models, in: International Symposium on Mixed and Augmented Reality, ISMAR ’07, Washington, DC, USA, 2007.

[7] B. Stenning, T. Barfoot, Path planning on a network of paths, in: Aerospace Conference, 2011 IEEE, 2011, pp. 1 –12.

[8] S. Se, H.-K. Ng, P. Jasiobedzki, T.-J. Moyung, Vision based modeling and localization for planetary exploration rovers, in: 55th International Astronautical Congress, 2004.

[9] A. Lambert, P. Furgale, T. Barfoot, J. Enright, Visual odometry aided by a Sun sensor and inclinometer, in: Aerospace Conference, 2011 IEEE, 2011, pp. 1 –14.
[10] D. Nistér, O. Naroditsky, J. Bergen, Visual odometry for ground vehicle applications, Journal of Field Robotics 23 (2006) 2006.
[11] R. Jiang, R. Klette, S. Wang, Modeling of unbounded long-range drift in visual odometry, in: Fourth Pacific-Rim Symposium on Image and Video Technology, 2010, pp. 121–126.
[12] G. Dubbelman, F. Groen, Bias reduction for stereo based motion estimation with applications to large scale visual odometry, in: International conference on Computer Vision and Pattern Recognition, 2009, pp. 1–8.
[13] G. Sibley, L. Matthies, G. Sukhatme, Bias reduction and filter convergence for long range stereo, in: S. Thrun, R. Brooks, H. Durrant-Whyte (Eds.), Robotics Research, Vol. 28 of Springer Tracts in Advanced Robotics, Springer Berlin / Heidelberg, 2007, pp. 285–294.
[14] R. Aragues, L. Carlone, G. Calafiore, C. Sagues, Multi-agent localization from noisy relative pose measurements, in: IEEE International Conference on Robotics and Automation (ICRA), 2011, pp. 364–369.
[15] B. Kim, M. Kaess, L. Fletcher, J. Leonard, A. Bachrach, N. Roy, S. Teller, Multiple relative pose graphs for robust cooperative mapping, in: International Conference on Robotics and Automation (ICRA), 2010, pp. 3185–3192.
[16] E. D. Nerurkar, S. I. Roumeliotis, A. Martinelli, Distributed maximum a posteriori estimation for multi-robot cooperative localization, in: IEEE International Conference on Robotics and Automation (ICRA), 2009, pp. 1402–1409.
[17] J. Knuth, P. Barooah, Distributed collaborative localization of multiple vehicles from relative pose measurements, in: 47th Annual Allerton Conference on Communication, Control, and Computing, Allerton, IL, 2009, pp. 314 –321. doi:10.1109/ALLERTON.2009.5394785.
[18] S. Su, C. S. G. Lee, Manipulation and propagation of uncertainty and verification of applicability of actions in assembly tasks, IEEE Transactions on Systems, Man, and Cybernetics 22 (6) (1982) 1376–1389.
[19] Y. Wang, G. S. Chirikjian, Error propagation on the euclidean group with applications to manipulator kinematics, IEEE Transactions on Robotics VOL. 22 (4) (2006) 1–12.
[20] Y. Wang, G. Chirikjian, Nonparametric-second order theory of error propagation on motion groups, International Journal of Robotics Research 27 (11-12) (2008) 1258–1273.
[21] Y. Zhou, G. S. Chirikjian, Probabilistic models of dead-reckoning error in nonholonomnic mobile robots, in: ICRA, 2003, pp. 1594–1599.
[22] P. Smith, T. Drummond, K. Roussopoulos, Computing MAP trajectories by representing, propagating and combining pdfs over groups, in: IEEE International Conference on Computer Vision, Vol. 2, 2003, pp. 1275–1282.
[23] J. Kwon, M. Choi, F. Park, C. Chun, Particle filtering on the euclidean group: framework and applications, Robotica 25 (2007) 725–737.
[24] M. Spong, S. Hutchinson, M. Vidyasagar, Robot Modeling and Control, John Wiley & Sons, Inc., 2006.
[25] G. Bleser, D. Strickera, Advanced tracking through efficient image processing and visual-inertial sensor fusion, Computers & Graphics 33 (1) (2009) 59–72. doi:DOI: 10.1016/j.cag.2008.11.004.
[26] B. Williams, M. Cummins, J. Neira, P. Newman, I. Reid, J. Tardós, A comparison of loop closing techniques in monocular SLAM, Robotics and Autonomous Systems 57 (2009) 1188–1197.
[27] Y. Ma, S. Soatto, J. Kosecka, S. S. Sastry, An invitation to 3-D vision, Interdisciplinary applied mathematics, Springer, 2006.
[28] K. Kanatani, Statistical optimization and geometric inference in computer vision [and discussion], Philosophical Transactions: Mathematical, Physical and Engineering Sciences 356 (1740) (1998) 1303–1320, (with R. Cipolla, R. I. Hartley, W. Triggs, A. Fitzgibbon, O. Faugeras in discussions).
[29] N. I. Fisher, T. Lewis, B. J. J. Embleton, Statistical Analysis of Spherical Data, Cambridge University Press, 1997.
[30] M. Fischler, L. Bolles, Random sample consensus: A paradigm for model fitting with applications to image analysis and automated cartography, Communications of the ACM 24 (1981) 381–385.
[31] R. Hartley, A. Zisserman, Multiple View Geometry in Computer Vision, Cambridge University Press, 2004.
[32] C. Tomasi, T. Kanade, Detection and tracking of point features, Tech. rep., Carnegie Mellon University (April 1991).

Appendix

Proof of Proposition 1. Let $\mathbf{y}$ be a d-dimensional random vector. Since $Cov(\mathbf{y},\mathbf{y}) = \mathrm{E}[\mathbf{y}\mathbf{y}^T] - \mathrm{E}[\mathbf{y}]\,\mathrm{E}[\mathbf{y}]^T$, we have upon taking the trace of both sides

$$\|\,\mathrm{E}[\mathbf{y}]\|^2 = \mathrm{E}[\|\mathbf{y}\|^2] - \mathrm{Tr}\,[Cov(\mathbf{y},\mathbf{y})] \leq \mathrm{E}[\|\mathbf{y}\|^2],$$

since $\mathrm{Tr}\,[Cov(\mathbf{y},\mathbf{y})] \geq 0$. Moreover equality in the above inequality holds if and only if the variance of each of the components of $\mathbf{y}$ is 0, that is, $\mathbf{y}$ is degenerate. We now apply this result to the random vector $\mathbf{y} := \mathbf{R}x$, where x is a deterministic d-dimensional vector while $\mathbf{R}$ is a random rotation matrix:

$$\|\,\mathrm{E}[\mathbf{R}]x\|^2 \leq \mathrm{E}[\|\mathbf{R}x\|^2] = \mathrm{E}[\|x\|^2] = \|x\|^2, \qquad (24)$$

where the first equality is due to the fact that rotation doesn't change the 2-norm of a vector, and the second equality is due to x being deterministic. This proves that $\|\,\mathrm{E}[\mathbf{R}]\| \leq 1$. Since $\mathbf{y}$ is degenerate if only if $\mathbf{R}$ is, the inequality in (24) is strict if $\mathbf{R}$ is non-degenerate. This proves the result.

The following additional technical result is needed for the proof of Lemma 1.

Proposition 2. *If X_i is a sequence of random vectors such that $\mathrm{E}[X_i^T X_j] \leq \overline{\alpha_0}\eta^{|i-j|}$, where $|\eta| < 1$ and $\overline{\alpha_0}$ is an arbitrary constant, then*

$$\mathrm{E}[(\sum_{i=1}^n X_i)^T(\sum_{i=1}^n X_i)] \leq \overline{\alpha_0}\frac{1+\eta}{1-\eta}n.$$

If in addition $\underline{\alpha_0}\eta^{|i-j|} \leq \mathrm{E}[X_i^T X_j]$ for $i \neq j$ and $0 < \beta_0 \leq \mathrm{E}[X_i^T X_i]$, where $\underline{\alpha_0}, \underline{\beta_0}$ are constants such that $\underline{\beta_0} > 2\frac{|\underline{\alpha_0}|}{1-|\eta|}$, then $\mathrm{E}[(\sum_{i=1}^n X_i)^T(\sum_{i=1}^n X_i)] = \Theta(n)$.

Proof of Proposition 2. Expanding the sum, we obtain

$$\mathrm{E}[(\sum_{i=1}^n X_i)^T(\sum_{i=1}^n X_i)] = \sum_{i=1}^n T_i, \qquad (25)$$

where

$$T_i := \sum_{j=1}^n \mathrm{E}[X_i^T X_j]. \qquad (26)$$

It follows from (26) and the hypothesis that

$$\begin{aligned}T_i &\le \overline{\alpha_0}(\eta^{i-1}+\eta^{i-2}+\cdots+\eta+1+\eta+\cdots+\eta^{n-i})\\ &= \overline{\alpha_0}(-1+\sum_{k=0}^{i-1}\eta^k+\sum_{k=0}^{n-i}\eta^k) \le \overline{\alpha_0}(-1+\sum_{k=0}^{\infty}|\eta|^k+\sum_{k=0}^{\infty}|\eta|^k)\\ &= \overline{\alpha_0}(-1+\frac{1}{1-|\eta|}+\frac{1}{1-|\eta|}) = \overline{\alpha_0}\frac{1+|\eta|}{1-|\eta|},\end{aligned}$$

where the second inequality follows from $|\eta| < 1$. The upper bound now follows from (25). This proves the first statement.

When the additional hypothesis holds, we have

$$\begin{aligned}T_i &\ge \underline{\alpha_0}(\eta^{i-1}+\eta^{i-2}+\cdots+\eta)+\underline{\beta_0}+\underline{\alpha_0}(\eta+\cdots+\eta^{n-i})\\ &\ge -2|\underline{\alpha_0}|\sum_{k=0}^{\infty}|\eta|^k+\underline{\beta_0} = \underline{\beta_0}-2\frac{|\underline{\alpha_0}|}{1-|\eta|} =: \ell_0 > 0\end{aligned}$$

It follows from (25) that $\mathrm{E}[(\sum_{i=1}^n X_i)^T(\sum_{i=1}^n X_i)] \ge n\ell_0 = \Omega(n)$. Combining the asymptotic lower and upper bounds, we get $\mathrm{E}[(\sum_{i=1}^n X_i)^T(\sum_{i=1}^n X_i)] = \Theta(n)$. ∎

Proof of Lemma 1. It follows from (4) that

$$\mathrm{E}[\hat{\mathbf{t}}^0_{0,n}] = \sum_{k=1}^{n}\mathrm{E}[\hat{\mathbf{t}}^0_{k,k+1}] \tag{27}$$

From (2)-(3) we get

$$\begin{aligned}\hat{\mathbf{t}}^0_{k,k+1} &= \mathbf{R}^0_1\tilde{\mathbf{R}}^0_1\ldots\mathbf{R}^k_{k+1}\tilde{\mathbf{R}}^k_{k+1}\left(\mathbf{t}^{k+1}_{k,k+1}+\tilde{\mathbf{t}}^{k+1}_{k,k+1}\right)\\ \Rightarrow \mathrm{E}[\hat{\mathbf{t}}^0_{k,k+1}] &= \mathbf{R}^0_k\,\overline{R}\ldots\mathbf{R}^k_{k+1}\left(\overline{R}\;\;\mathbf{t}^{k+1}_{k,k+1}+\boldsymbol{\rho}_{k+1}\right)\end{aligned}$$

where the second equality follows from the assumption that the orientation measurement errors are i.i.d. Since a rotation does not change the 2-norm of a vector,

$$\|\,\mathrm{E}[\hat{\mathbf{t}}^0_{k,k+1}]\| \le \|\overline{R}^k\|\left(\|\overline{R}\|\;\;\|\mathbf{t}^{k+1}_{k,k+1}\|+\|\boldsymbol{\rho}_{k+1}\|\right)$$

where the inequality follows from applying triangle inequality and using sub-multiplicative property of induced norms. Since $\|\overline{R}^k\| \le \|\overline{R}\|^k$, we obtain upon using Proposition 1 and the definition $\gamma = \|\overline{\mathbf{R}}\|$ that

$$\|\,\mathrm{E}[\hat{\mathbf{t}}^0_{k,k+1}]\| \le \gamma^k a,$$

where $a := \sup_k(\|\overline{R}\|\|\mathbf{t}^{k+1}_{k,k+1}\|+\|\boldsymbol{\rho}_{k+1}\|) \le \gamma\tau+\beta$. Applying triangle inequality to (27), we get

$$\|\,\mathrm{E}[\hat{\mathbf{t}}^0_{0,n}]\| \le \sum_{k=0}^{n-1}\|\,\mathrm{E}[\hat{\mathbf{t}}^0_{k,k+1}]\| \quad \le a\sum_{k=0}^{n-1}\gamma^k \le a\frac{1-\gamma^n}{1-\gamma},$$

since $0 < \gamma < 1$. This proves the result about the mean.

The proof for the second moment result proceeds by first showing that $\mathrm{E}[(\hat{\mathbf{t}}^0_{j,j+1})^T\hat{\mathbf{t}}^0_{i,i+1}]$ satisfies the hypothesis of Proposition 2 and then applying the proposition. We note that for $i \le j$,

$$\begin{aligned}(\hat{\mathbf{t}}^0_{i,i+1})^T\hat{\mathbf{t}}^0_{j,j+1} &= (\hat{\mathbf{t}}^{i+1}_{i,i+1}\hat{\mathbf{R}}^0_{i+1})^T\,\hat{\mathbf{R}}^0_{j+1}\hat{\mathbf{t}}^{j+1}_{j,j+1}\\ &= (\hat{\mathbf{t}}^{i+1}_{i,i+1})^T\,\hat{\mathbf{R}}^{i+1}_{j+1}\,\hat{\mathbf{t}}^{j+1}_{j,j+1}\\ &= V_1+V_2+V_3+V_4,\end{aligned}$$

where

$$\begin{aligned}V_1 &:= (\mathbf{t}^{i+1}_{i,i+1})^T\;\;\hat{\mathbf{R}}^{i+1}_{j+1}\;\;\mathbf{t}^{j+1}_{j,j+1}\\ V_2 &:= (\tilde{\mathbf{t}}^{i+1}_{i,i+1})^T\;\;\hat{\mathbf{R}}^{i+1}_{j+1}\;\;\mathbf{t}^{j+1}_{j,j+1}\\ V_3 &:= (\mathbf{t}^{i+1}_{i,i+1})^T\;\;\hat{\mathbf{R}}^{i+1}_{j+1}\;\;\tilde{\mathbf{t}}^{j+1}_{j,j+1}\\ V_4 &:= (\tilde{\mathbf{t}}^{i+1}_{i,i+1})^T\;\;\hat{\mathbf{R}}^{i+1}_{j+1}\;\;\tilde{\mathbf{t}}^{j+1}_{j,j+1}.\end{aligned}$$

We now evaluate the expected values of these four terms. By using the Independence of the orientation measurement errors and, we get

$$\begin{aligned}\mathrm{E}[V_1] &= (\mathbf{t}^{i+1}_{i,i+1})^T\;\;\mathbf{R}^{i+1}_{i+2}\overline{R}\ldots\mathbf{R}^j_{j+1}\overline{R}\;\;\mathbf{t}^{j+1}_{j,j+1}\\ \Rightarrow |\,\mathrm{E}[V_1]| &\le \|\mathbf{t}^{i+1}_{i,i+1}\|\,\|\overline{R}^{j-i}\;\mathbf{t}^{j+1}_{j,j+1}\|\\ &\le \|\overline{R}^{j-i}\|\,\|\mathbf{t}^{i+1}_{i,i+1}\|\,\|\mathbf{t}^{j+1}_{j,j+1}\| \le \gamma^{j-i}\tau^2,\end{aligned}$$

where the first inequality uses the fact that rotations do not change the 2-norm. For V_2, since $\tilde{\mathbf{t}}^{i+1}_{i,i+1}$ is statistically dependent only on $\tilde{\mathbf{R}}^i_{i+1}$ and not on $\tilde{\mathbf{R}}^{i+1}_{i+2}, \ldots, \tilde{\mathbf{R}}^j_{j+1}$, it is also independent of $\hat{\mathbf{R}}^{i+1}_{j+1}$. Hence,

$$|\,\mathrm{E}[V_2]| = |\mathbf{b}_i\;\mathbf{R}^{i+1}_{i+2}\;\overline{R}\mathbf{R}^j_{j+1}\;\overline{R}\mathbf{t}^{j+1}_{j,j+1} \quad \Rightarrow \quad |\,\mathrm{E}[V_2]| \le \gamma^{j-i}\,b\tau.$$

Similarly, we have, for $i < j$,

$$\begin{aligned}\mathrm{E}[V_3] &= (\mathbf{t}^i_{i+1,i+1})^T\;\mathbf{R}^{i+1}_{j+1}\;\overline{R}\;\mathbf{R}^{j-1}_j\overline{R}\;\boldsymbol{\rho}_{j+1}\\ \Rightarrow |\,\mathrm{E}[V_3]| &\le \gamma^{j-i}\frac{1}{\gamma}\tau\rho.\end{aligned}$$

and for $i = j$, $|\,\mathrm{E}[V_3]| \le \tau b$. For V_4, when $i < j$, we have

$$\begin{aligned}V_4 &= (\tilde{\mathbf{t}}^{i+1}_{i,i+1})^T\;\mathbf{R}^{i+1}_{i+2}\;\tilde{\mathbf{R}}^{i+1}_{i+2}\ldots\mathbf{R}^j_{j+1}\;\tilde{\mathbf{R}}^j_{j+1}\;\tilde{\mathbf{t}}^{j+1}_{j,j+1},\\ \Rightarrow |\,\mathrm{E}[V_4]| &\le \|\mathbf{b}_i\|\,\|\overline{\mathbf{R}}\|^{j-i-1}\|\boldsymbol{\rho}_{j+1}\| \le \gamma^{j-i}\frac{1}{\gamma}b\rho.\end{aligned}$$

When $i = j$, we have $V_4 = (\tilde{\mathbf{t}}^{j+1}_{j,j+1})^T\;\tilde{\mathbf{t}}^{j+1}_{j,j+1}$, which implies $\mathrm{E}[V_4] = \mathrm{Tr}\,[\mathbf{P}_{j+1}] + \mathbf{b}^T_{j+1}\mathbf{b}_{j+1}$, by definition. Therefore,

$$0 < \underline{p} \le \mathrm{E}[V_4] \le \overline{p}+b^2. \quad (i=j).$$

Combining all four terms, we get,

$$\begin{aligned}\underline{\alpha_0}\gamma^{j-i} \le \mathrm{E}[(\hat{\mathbf{t}}^0_{i,i+1})^T\hat{\mathbf{t}}^0_{j,j+1}] &\le \alpha_0\gamma^{j-i}, \quad (i<j)\\ \underline{\beta_0} \le \mathrm{E}[(\hat{\mathbf{t}}^0_{i,i+1})^T\hat{\mathbf{t}}^0_{i,i+1}] &\le \beta_0,\end{aligned}$$

where $\underline{\alpha_0} := -(\tau^2+\tau b+\frac{1}{\gamma}\tau\rho+\frac{1}{\gamma}b\rho)$, $\alpha_0 := \tau^2+\tau b+\frac{1}{\gamma}\tau\rho+\frac{1}{\gamma}b\rho$, and $\underline{\beta_0} := \underline{p}-(\tau^2+2\tau b)$, $\beta_0 := \tau^2+2\tau b+\overline{p}+b^2$. Note

that in case $\underline{\beta_0}$ is negative, it is a poor lower lower bound since $(\hat{\mathbf{t}}^0_{i,i+1})^T\hat{\mathbf{t}}^0_{i,i+1} > 0$. Repeating these arguments for $i \geq j$ and combining, we find that

$$\underline{\alpha_0}\gamma^{|i-j|} \leq \mathrm{E}[(\hat{\mathbf{t}}^0_{i,i+1})^T\hat{\mathbf{t}}^0_{j,j+1}] \leq \overline{\alpha_0}\gamma^{|i-j|}, \quad (i \neq j)$$
$$\max\{0, \underline{\beta_0}\} \leq \mathrm{E}[(\hat{\mathbf{t}}^0_{i,i+1})^T\hat{\mathbf{t}}^0_{i,i+1}] \leq \overline{\alpha_0},$$

where $\overline{\alpha_0} := \max\{\alpha_0, \beta_0\}$. Now call $X_i := \hat{\mathbf{t}}^0_{i,i+1}$, so that $\hat{\mathbf{t}}^0_{0,n} = \sum_{i=0}^{n-1} X_i$. Hence, $\mathrm{E}[(\hat{\mathbf{t}}^0_{0,n})^T\hat{\mathbf{t}}^0_{0,n}] = \mathrm{E}[(\sum_{i=0}^{n-1} X_i)^T(\sum_{j=0}^{n-1} X_j)]$. It now follows from Proposition 2 that $\mathrm{E}[(\hat{\mathbf{t}}^0_{0,n})^T\hat{\mathbf{t}}^0_{0,n}]$ is $O(n)$, and is $\Theta(n)$ if $\underline{\beta_0} > 2\frac{|\underline{\alpha_0}|}{1-\gamma}$. Since $|\underline{\alpha_0}| = \tau^2+\tau b+\tau\rho$, the condition $\underline{\beta_0} > 2\frac{|\underline{\alpha_0}|}{1-\gamma}$ is equivalent to $\underline{p} > 2b\tau + \tau^2 + 2\dfrac{(\tau+\rho/\gamma)(\tau+b)}{1-\gamma}$, which proves the result. ∎

Proof of Theorem 2. Define a new random variable, $\delta\tilde{\theta}_{k-1,k} := \tilde{\theta}_{k-1,k} - \mathrm{E}[\tilde{\theta}_{k-1,k}]$. Then $\{\delta\tilde{\theta}_{k-1,k}\}_{k=0}^{\infty}$ is an i.i.d. sequence and the marginal density of $\delta\tilde{\theta}_{k-1,k}$ is symmetric about 0. We define the corresponding rotation matrices $\delta\tilde{R}^i_j := f_R(\delta\tilde{\theta}_{i,j})$. Utilizing the commutative property of 2-D rotation matrices, we have $\tilde{\mathbf{R}}^i_j = \left(\underline{\mathbf{R}}^{j-i}\right)\delta\tilde{R}^i_j$. It then follows from (5) that

$$\mathbf{e}(n) = n\mathbf{r} - \hat{\mathbf{t}}^0_{0,n}$$

and from (4), (3), and (2) that

$$\hat{\mathbf{t}}^0_{0,n} = \sum_{k=1}^{n}\left(\prod_{i=1}^{k}\underline{\mathbf{R}}\delta\tilde{R}^{i-1}_i\right)\left(\mathbf{r} + \tilde{\mathbf{t}}^k_{k-1,k}\right),$$

where we have used the fact that $\hat{\mathbf{R}}^{i-1}_i = \mathbf{R}^{i-1}_i\tilde{\mathbf{R}}^{i-1}_i = \underline{\mathbf{R}}\delta\tilde{R}^{i-1}_i$ since $\mathbf{R}^{i-1}_i = I$ due to the nature of the trajectory. We define two new random variables

$$\mathbf{f}_n := \sum_{k=1}^{n}\left(\prod_{i=1}^{k}\underline{\mathbf{R}}\delta\tilde{R}^{i-1}_i\right)\mathbf{r}$$
$$\mathbf{g}_n := \sum_{k=1}^{n}\left(\prod_{i=1}^{k}\underline{\mathbf{R}}\delta\tilde{R}^{i-1}_i\right)\tilde{\mathbf{t}}^k_{k-1,k},$$

so that

$$\hat{\mathbf{t}}^0_{0,n} = \mathbf{f}_n + \mathbf{g}_n. \tag{28}$$

By the i.i.d. assumption on the sequence $\{\tilde{\theta}_{k-1,k}\}_k$, the sequence $\{\delta\tilde{R}^{k-1}_k\}_k$ is also i.i.d., so that

$$\mathrm{E}[\delta\tilde{R}^i_j] = \mathrm{E}[\prod_{k=i+1}^{k}\delta\tilde{R}^{k-1}_k] = \prod_{k=i-1}^{j}\mathrm{E}[\delta\tilde{R}^{k-1}_k] = c^{j-i}I, \tag{29}$$

where we have used the fact that $\mathrm{E}[\sin\delta\tilde{\theta}_{i-1,i}] = 0$, which follows from Assumption 1. It is then straightforward to show that

$$\mathrm{E}[\mathbf{f}_n] = \sum_{k=1}^{n}(c\underline{\mathbf{R}})^k\,\mathbf{r} = (I - c\underline{\mathbf{R}})^{-1}\left(I - (c\underline{\mathbf{R}})^n\right)c\underline{\mathbf{R}}\mathbf{r}$$
$$\mathrm{E}[\mathbf{g}_n] = \sum_{k=0}^{n-1}(c\underline{\mathbf{R}})^k\,\boldsymbol{\rho} = (I - c\underline{\mathbf{R}})^{-1}\left(I - (c\underline{\mathbf{R}})^n\right)\boldsymbol{\rho}$$

The expected value $\mathbf{e}(n)$ is now

$$\mathrm{E}[\mathbf{e}(n)] = n\,\mathbf{r} - (I - c\underline{\mathbf{R}})^{-1}\left(I - (c\underline{\mathbf{R}})^n\right)(c\underline{\mathbf{R}}\mathbf{r} + \boldsymbol{\rho}) \tag{30}$$

which proves the first equality in (18).

For the variance, it follows from (28) that

$$\begin{aligned}\mathrm{Tr}\left[Cov(\mathbf{e}(n), \mathbf{e}(n))\right] &= \mathrm{Tr}\left[Cov(\hat{\mathbf{t}}^0_{0,n}, \hat{\mathbf{t}}^0_{0,n})\right] \\ &= \mathrm{E}[\mathbf{f}_n^T\mathbf{f}_n] + \mathrm{E}[\mathbf{g}_n^T\mathbf{g}_n] + 2\,\mathrm{E}[\mathbf{f}_n^T\mathbf{g}_n] \\ &\quad - \mathrm{E}[\hat{\mathbf{t}}^0_{0,n}]^T\,\mathrm{E}[\hat{\mathbf{t}}^0_{0,n}].\end{aligned} \tag{31}$$

$$\begin{aligned}\mathrm{E}[\mathbf{f}_n^T\mathbf{f}_n] &= \mathbf{r}^T\,\mathrm{E}\left[\sum_{i=1}^{n}\left(\prod_{j=1}^{i}\underline{\mathbf{R}}\,\delta\tilde{R}^{j-1}_j\right)^T\sum_{k=1}^{n}\left(\prod_{\ell=1}^{k}\underline{\mathbf{R}}\,\delta\tilde{R}^{\ell-1}_\ell\right)\right]\mathbf{r} \\ &= \mathbf{r}^T\Big[\left(I + c\underline{\mathbf{R}}^T + \cdots + (c\underline{\mathbf{R}}^T)^{n-1}\right) \\ &\quad + \left(c\underline{\mathbf{R}} + I + c\underline{\mathbf{R}}^T + \cdots + (c\underline{\mathbf{R}}^T)^{n-2}\right) \\ &\quad \cdots + \left((c\underline{\mathbf{R}})^{n-1} + \cdots + I\right)\Big]\mathbf{r}\end{aligned}$$

where we have used the independence of the sequence $\{\delta\tilde{R}^{k-1}_k\}_k$ and the fact that $\delta\tilde{R}^{k-1}_k\delta\tilde{R}^{k-1}_k = I = \underline{\mathbf{R}}\,\underline{\mathbf{R}}^T$. The expression above simplifies to

$$\begin{aligned}\mathrm{E}[\mathbf{f}_n^T\mathbf{f}_n] &= \mathbf{r}^T\left[nI + 2\sum_{k=1}^{n-1}(n-k)\,(c\underline{\mathbf{R}})^k\right]\mathbf{r} = \mathbf{r}^T\,(I - c\underline{\mathbf{R}})^{-2} \\ &\quad \times\left(I + 2(n-2)c\underline{\mathbf{R}} - 2(n-1)\,(c\underline{\mathbf{R}})^2 + 2\,(c\underline{\mathbf{R}})^{n+1}\right)\mathbf{r}.\end{aligned}$$

To examine $\mathrm{E}[\mathbf{g}_n^T\mathbf{g}_n]$, we express the product as $\mathbf{g}_n^T\mathbf{g}_n = \sum_{k=1}^{n}T_k$ where

$$\begin{aligned}T_k &= (\tilde{\mathbf{t}}^k_{k-1,k})^T\left((\delta\tilde{R}^{k-1}_k)^T\ \ (\delta\tilde{R}^{k-2}_{k-1})^T\ldots(\delta\tilde{R}^0_1)^T\right)(\underline{\mathbf{R}}^k)^T \\ &\quad\times\left(\underline{\mathbf{R}}\ \ \delta\tilde{R}^0_1\tilde{\mathbf{t}}^1_{0,1} + \cdots + \underline{\mathbf{R}}^n\ \delta\tilde{R}^0_1\ldots\delta\tilde{R}^{k-1}_k\tilde{\mathbf{t}}^k_{k-1,k}\right).\end{aligned}$$

Taking expectation and using the assumptions on the noise correlations, we get for $k > 1$,

$$\begin{aligned}\mathrm{E}[T_k] &= \mathrm{Tr}\left[P + \mathbf{b}\mathbf{b}^T\right] + \mathbf{b}^T((c\underline{\mathbf{R}})^{k-2} + (c\underline{\mathbf{R}})^{k-3} + \cdots + I \\ &\quad + I + (c\underline{\mathbf{R}}) + (c\underline{\mathbf{R}})^2 + \cdots + (c\underline{\mathbf{R}})^{n-1-k})\boldsymbol{\rho},\end{aligned}$$

and for $k = 1$, $\mathrm{E}[T_k] = \mathrm{Tr}\left[\mathbf{P} + \mathbf{b}\mathbf{b}^{\mathbf{T}}\right] + \mathbf{b}^T(I + c\underline{\mathbf{R}} + (c\underline{\mathbf{R}})^2 + \cdots + (c\underline{\mathbf{R}})^{n-1-k})\boldsymbol{\rho}$. Repeating this for all the T_k's we get:

$$\begin{aligned}\mathrm{E}[\mathbf{g}_n^T\mathbf{g}_n] &= n\,\mathrm{Tr}\left[\mathbf{P} + \mathbf{b}\mathbf{b}^T\right] + \mathbf{b}^T\left[2\sum_{k=0}^{n-2}(n-k-1)\,(c\underline{\mathbf{R}})^k\right]\boldsymbol{\rho} \\ &= n\,\mathrm{Tr}\left[\mathbf{P} + \mathbf{b}\mathbf{b}^T\right] + \mathbf{b}^T\,(I - c\underline{\mathbf{R}})^{-2}\times \\ &\quad [2(n-1)I - 2nc\underline{\mathbf{R}} + 2\,(c\underline{\mathbf{R}})^n]\,\boldsymbol{\rho}.\end{aligned}$$

Similar tedious calculations lead to the following

$$\begin{aligned}\mathrm{E}[\mathbf{f}_n^T\mathbf{g}_n] &= \left[\sum_{k=0}^{n-1}\mathbf{b}^T(c\underline{\mathbf{R}})^k + \sum_{k=0}^{n-2}(n-k-1)\boldsymbol{\rho}^T(c\underline{\mathbf{R}}^T)^k\right]\mathbf{r} \\ &= \mathbf{b}^T\left(I-c\underline{\mathbf{R}}\right)^{-2}\left[I-c\underline{\mathbf{R}}-(c\underline{\mathbf{R}})^n+(c\underline{\mathbf{R}})^{n+1}\right]\mathbf{r} \\ &\quad + \mathbf{r}^T\left(I-c\underline{\mathbf{R}}\right)^{-2}\left[(n-1)I-nc\underline{\mathbf{R}}+(c\underline{\mathbf{R}})^n\right]\boldsymbol{\rho}.\end{aligned}$$

Plugging all of this back in (31), we get $\mathrm{Tr}\left[Cov\left(\mathbf{e}(n),\mathbf{e}(n)\right)\right] = \psi n + \omega(n)$, where $\psi, \omega(n)$ are given in (15). This proves the second equality in (18). ■

Proof of Theorem 3. Define a new random variable, $\delta\tilde{\theta}_{k-1,k} := \tilde{\theta}_{k-1,k} - \mathrm{E}[\tilde{\theta}_{k-1,k}]$. The sequence $\{\delta\tilde{\theta}_{k-1,k}\}_{k=0}^{\infty}$ are then i.i.d. and the marginal density of $\delta\tilde{\theta}_{k-1,k}$ is symmetric about the origin for each k. We define the corresponding rotation matrices $\delta\tilde{R}_j^i := f_R(\delta\tilde{\theta}_{i,j})$. Utilizing the commutative property of rotations in 2-D, we have the following relation

$$\tilde{\mathbf{R}}_j^i = \left(\underline{\mathbf{R}}^{j-i}\right)\delta\tilde{R}_j^i \tag{32}$$

To examine the bias, we first re-write the position estimate $\hat{\mathbf{t}}_{0,n}^0$ as

$$\begin{aligned}\hat{\mathbf{t}}_{0,n}^0 = \sum_{i=0}^{n}\hat{\mathbf{t}}_{i,i+1}^0 &= \sum_{k=0}^{\eta-1}\left(\sum_{m=1}^{p}\hat{\mathbf{t}}_{kp+m-1,kp+m}^0\right) \\ &\quad + \sum_{j=1}^{q}\hat{\mathbf{t}}_{\eta p+j-1,\eta p+j}^0,\end{aligned} \tag{33}$$

where the first term is sum is over all time steps up to the end of the last (η-th) period and the second term for the time steps after that. For any $0 \le m < p$, we have

$$\begin{aligned}\hat{\mathbf{t}}_{kp+m-1,kp+m}^0 &= \hat{\mathbf{R}}_{kp+m}^0\ \hat{\mathbf{t}}_{kp+m-1,kp+m}^{kp+m} \\ &= \mathbf{R}_m^0\ \tilde{\mathbf{R}}_{kp+m}^0(\mathbf{t}_{m-1,m}^m + \tilde{\mathbf{t}}_{kp+m-1,kp+m}^{kp+m}),\end{aligned}$$

where apart from $\hat{R} = R\tilde{R}$, we have used the periodic nature of the trajectory that leads to $\mathbf{R}_{kp+m}^0 = \mathbf{R}_m^0$ and $\mathbf{t}_{kp+m-1,kp+m}^{kp+m} = \mathbf{t}_{m-1,m}^m$. Taking expectation and using (32), we obtain

$$\mathrm{E}[\hat{\mathbf{t}}_{kp+m-1,kp+m}^0] = \mathbf{R}_m^0(c\underline{\mathbf{R}})^{kp+m-1}(c\underline{\mathbf{R}}\mathbf{t}_{m-1,m}^m + \boldsymbol{\rho}_m)$$

This expression is used to evaluate $\mathrm{E}[\mathbf{t}_{0,n}^0]$ by taking expectation of the right hand side of (33). After grouping terms, we obtain

$$\mathrm{E}[\mathbf{t}_{0,n}^0] = \left(\sum_{k=0}^{\eta-1}(c\underline{\mathbf{R}})^{kp}\omega(p)\right) + (c\underline{\mathbf{R}})^{\eta p}\omega(q) \tag{34}$$

Using techniques similar to those used in the proof of Theorem 2, it can be shown that

$$\begin{aligned}\mathrm{E}[\hat{\mathbf{t}}_{0,n}^0] &= \sum_{i=0}^{\eta-1}(c\underline{\mathbf{R}})^{ip}w + (c\underline{\mathbf{R}})^{\eta p}w(q) \\ \Rightarrow \mathrm{E}[\mathbf{e}(n)] &= \sum_{k=0}^{q-1}\mathbf{R}_{k+1}^0\mathbf{t}_{k,k+1}^{k+1} - \sum_{k=0}^{\eta-1}(c\underline{\mathbf{R}})^{kp}w - (c\underline{\mathbf{R}})^{\eta p}w(q).\end{aligned}$$

By replacing the summation we arrive at (20). ■